DETERMINATION OF THE DYNAMIC RESPONSE OF BRIDGES FROM ACCELEROMETER DATA

By

MIGUEL BELTRAN

A thesis submitted to the

Graduate School – New Brunswick

in part fulfillment of the requirements

for the degree of

Master of Science

Graduate Program in Civil and Environmental Engineering

written under the direction of

Dr. Hani H. Nassif

and approved by

_____

_____

_____

New Brunswick, New Jersey

May 2013

ABSTRACT OF THE THESIS

Determination of the Dynamic Response of Bridges from Accelerometer Data

by MIGUEL BELTRAN

Thesis Director:

Dr. Hani H. Nassif

Debonding of reinforcement in highway bridge decks can result from vibrations induced by large vehicular live loads in adjacent lanes. These detrimental effects can be evaluated by comparing rebar vibrations during concrete setting to experimentally established limits in terms of peak particle velocity. However, methods of directly measuring rebar velocity are limited. It is often more feasible to process accelerometer measurements to obtain velocity data indirectly, but common processing techniques such as direct integration will produce errors due to unknown, non-zero initial values combined with random noise on the structure. Using a combination of numerical and subjective analyses to mitigate the various sources of error, an approach is developed to estimate velocities and displacements from raw accelerometer data. Initial calibration of the algorithm is achieved by conducting a comprehensive field testing program for two independent highway bridges. The estimated dynamic response of the bridge girders compare well with the measurements taken by a Laser Doppler Vibrometer in the field.

In most cases, the time histories of velocity and displacement are accurately predicted by the algorithm.

The response of a bridge superstructure is monitored for an extended period, encompassing the pour of two full spans and several hours after initial concrete placement. The investigation is performed systematically; starting with the girders, progressing to the bridge deck, and culminating in the determination of rebar velocity relative to the surrounding concrete deck. Comparison with established vibration limits suggests that the vibrations during the concrete initial setting period should not pose any significant risk of debonding.

ACKNOWLEDGEMENTS

I would like to thank Dr. Hani H. Nassif for his guidance and encouragement. The constant challenges he has provided for me have helped me grow by leaps and bounds as both an intellectual and a human being.

I would also like to thank Dr. Kaan Ozbay and Dr. Hao Wang for serving on my committee. Their knowledgeable advice and recommendations were key contributions in this work.

I would like to thank my mother and sister for their unwavering support throughout my education. I could not have achieved anything in my life without the countless sacrifices they have made for me.

I would like to thank my Uncle Arthur, for bringing me into his family and ensuring me that I will always have a home away from home.

I would like to thank my friends, Mussie Eyob, Herbert Silva, Ci Zheng, Min Li, and Scott Wu. When I was at my lowest, you guys picked me up and showed me the important things in life. You will always be my friends.

I would like to thank Dan Su for always extending a helping hand. He has never shown any hesitation in putting his own interests aside and sharing his knowledge with myself and my colleagues.

I would like to thank Khalid Machich, Peng Lou, Ye Xia, Michael Salvador, Adi Abu-Obeidah, Jonathan Eagelton, and all of my colleagues for transforming the workplace into a place of community, warmth, and merriment each and every day.

Table of Contents

List of Figures

List of Tables

CHAPTER 1

INTRODUCTION

1.1 PROBLEM STATEMENT

Cracking of reinforced concrete bridge decks is a major concern in the bridge industry. This exposes the deck reinforcement to corrosion, jeopardizing the integrity of the structure. An aspect of structural health less explored is the possibility of debonding of the steel reinforcement from the surrounding concrete. Debonding can result from improper cleaning of reinforcement. In staged construction or rehabilitation projects, vibrations in freshly placed deck concrete induced by adjacent truck traffic can also weaken rebar bond. Even without any risk of corrosion, significant debonding of the reinforcement will be detrimental to the structures. In either case of rebar corrosion or debonding, the reinforcement is unable to intercept cracks as they propagate through the depth of the deck. Therefore, it is vital in the evaluation of the health of bridges to monitor vibrations on freshly placed deck concrete.

While debonded reinforcement becomes a concern for the cracked deck condition, it is also important to address the actual causes of cracking. One method of assessing bridge performance and serviceability is to monitor bridge deflections. In the past, contact sensors such as linear variable differential transformers (LVDT's) and non-contact sensors such as laser Doppler vibrometers (LDV's) have been used to measure displacements, but installation of either of these sensors can be difficult and often

impractical. Accelerometers, on the other hand, are comparatively inexpensive, durable, and easy to install. Given that acceleration, velocity, and displacement are all closely related, the rebar velocities and bridge displacements can be monitored using just accelerometers.

The integration of acceleration data to estimate velocity and displacement, though widely practiced, is a complicated process riddled with errors. Factors such as instrument drift, unknown initial conditions, and random noise can result in significant errors in the estimated velocities and displacements. As computational technology improved, so did the integration techniques and correction methods. Still, no single algorithm has been shown to give consistently accurate results for a wide variety of acceleration signals.

1.2 RESEARCH OBJECTIVE AND SCOPE

In this study, the dynamic responses are evaluated for two bridges: the NJTA Interchange 7A Bridge (Structure No. 60.51I) and the Hackensack River Lewandowski Memorial Bridge (Structure No. E109.83). A method is developed to predict velocity and displacement time-histories from accelerometer data, and the algorithm is validated by comparing the estimated velocities and displacements with experimentally measured values. Ultimately, the corrected algorithm is used to evaluate the dynamic response of the deck reinforcement bars during concrete placement to determine if debonding is a legitimate concern in staged construction projects.

1.3 THESIS ORGANIZATION

This thesis is composed of six chapters organized in the following manner:

Chapter 1 presents the problem and summarizes the solution proposed in the study.

Chapter 2 gives a full discussion on the existing literature that helped guide the study. Previous works on rebar debonding are explained in brief, but the majority of the discussion pertains to signal processing techniques and applications.

Chapter 3 gives a detailed explanation of the experimental program conducted in the study and the desired outcomes of the work. The instrumentation of the 7A Bridge and Hackensack Bridge are carefully illustrated to provide sufficient details to reproduce the experiment.

Chapter 4 focuses on the methodology and rational approach. It provides a bridge between the experimental procedure and the final results that are pursued in the study. A detailed procedure is given for converting raw accelerometer data into velocity and displacement. Preliminary results are included to fully demonstrate the concepts discussed throughout the chapter.

Chapter 5 provides a comprehensive analysis of the results from the experimental and numerical investigations. The results for each of the two bridges are discussed separately.

Chapter 6 contains the summary and conclusions. A discussion on future research highlights the important aspects of the study that need to be explored in greater detail.

CHAPTER 2

LITERATURE REVIEW

2.1 VIBRATION EFFECTS ON EARLY AGE CONCRETE

Concrete properties are very sensitive at the early age. For example, the strength in the concrete is affected by the proper development of bond between the cement paste and aggregate. Similarly, the bond strength between the paste and rebar is essential to the performance of reinforced concrete. These factors are strongly influenced by the conditions under which the concrete is allowed to age, and disturbance to the concrete in the form of vibration during early age can cause severe damage. Altowaiji et al. (1986) investigated the effects of internal revibration on the bond between concrete and steel reinforcement to determine whether or not the industry practice was beneficial. It was found that revibration after 45 and 90 minutes significantly reduced the bond strength for bottom-cast bars when using low-slump concrete, while it increased the bond strength for top-cast bars with high-slump concrete. However, the gains in bond strength for the top-cast bars did not outweigh the detrimental effects on bottom-cast bars. The effects of external revibration were studied by Harsh and Darwin (1986) by simulating traffic induced vibrations. Results showed that these vibrations were detrimental to the concrete-steel bond only when slumps were above 3 to 4 inches. Nassif et al. (2007) performed field tests on the Delaware River Turnpike Bride and found that adjacent traffic had adverse effects on both the paste-aggregate and paste-rebar bonds.

Given these findings, unnecessary vibrations on fresh concrete should be limited. Hulshizer and Desai (1984) attempted to establish specific shock vibration limits in terms of peak particle velocity. In the study, concrete strength and rebar pullout tests were performed on specimens subjected to different magnitudes of vibration. Although the researchers applied vibrations with peak particle velocities more than 16 inches per second (representative of a large explosion), they were unable to find a vibration threshold at which significant reductions in compressive or pullout strength could be expected. Nevertheless, conservative recommendations were given to limit shock vibrations on concrete and various ages, which are summarized in Table 2.1.

Table 2.1 Vibration limits on freshly placed concrete (Hulshizer and Desai, 1984)

Age of concrete at time of vibration (hours)	Peak particle velocity
0-3	102 mm/sec (4.0 in/sec)
3-11	38 mm/sec (1.5 in/sec)
11-24	51 mm/sec (2 in/sec)
24-48	102 mm/sec (4.0 in/sec)
48+	178 mm/sec (7.0 in/sec)

2.2 ESTIMATION OF DISPLACEMENT SIGNAL FROM ACCELEROMETER DATA

From physics, there is a close relationship between acceleration, velocity, and displacement. While it is straightforward to twice differentiate a time history of displacement to obtain acceleration, it is significantly more difficult to accurately predict displacement by double integrating acceleration. Part of the incompatibility is due to transducer errors. Along with the DC offsets that exist in all transducers, there are also errors and information loss during discretization and quantization that are amplified during double integration (Gilbert et al., 2010). Unknown initial conditions also result in an offset and drift that can be essentially treated in the same manner as DC offsets (Ribeiro et al., 2002). Lastly, very low frequency noise can cause solutions to diverge due to the conversion factor of $1/f$ involved in integration of acceleration and velocity signals (Arraigada and Partl, 2006). Consequently, much of the studies performed on acceleration signal processing seek to overcome one or more of these error sources, whereas the choice of conversion method is often reduced to either time domain or frequency domain analysis.

2.2.1 Conversion in the Time Domain

Direct integration in the time domain involves the calculation of the area under a continuous function $a(t)$ or the corresponding discretized time history. Numerical methods such as Simpson's rule or the trapezoidal method are commonly used. For high sampling rates where the sampling interval, Δt is small, the trapezoidal method is sufficiently accurate compared to other methods. Therefore, the discussions on time

integration in this study will assume that the trapezoidal method is used. From Arraigada and Partl (2006), the formula for integration in this manner is given by:

$$\int_0^n a(t)dt = \sum_{i=1}^{n}\left(\frac{a(i-1)+a(i)}{2}\right)\Delta t \tag{2.1}$$

where:

a(t): continuous time wave form

a(i): *i*th sample of the time waveform

Δt: time increment between samples

n: total number of samples

This numerical approximation becomes more accurate for signals with low curvature and for high sampling rates. When integrating the acceleration to estimate velocity, the bias error of the trapezoidal method is given by Han and Chung (2002) as:

$$E = \frac{\Delta t^3}{12} a(t) \tag{2.2}$$

Given this expression, it is apparent that error can be dramatically reduced by increasing the sampling frequency. The researchers further show that:

$$f_s = \left(\frac{3\varepsilon}{2\pi^3}\right)^{-1/3} f_o \tag{2.3}$$

where:

f_s: sampling frequency of the signal

f_o: actual frequency of vibration

For example, to estimate velocity within 5 percent error using direct integration, the minimum sampling frequency required is 7.45 f_o. For 1 percent error, the minimum f_s required is 12.74 f_o.

Unknown initial conditions can also produce significant errors. Gindy et al. (2007) show the following relationships between acceleration, velocity, and displacement with non-zero initial conditions:

$$v(t) = v_o + \int_{t_1}^{t_2} a(t)dt \tag{2.4}$$

$$x(t) = x_o + \int_{t_1}^{t_2} v(t)dt = x_o + v_o t + \int_{t_1}^{t_2}\int_{t_1}^{t_2} a(t)dt \tag{2.5}$$

where:

a(t): acceleration with respect to time

v(t): velocity with respect to time

x(t): displacement with respect to time

v_o: initial velocity

x_o: initial displacement

Integration of an acceleration signal while assuming zero initial conditions will result in an offset of $-v_o$ in the velocity estimate, and an offset of $-x_o$ combined with a drift of slope $-v_o$ in the displacement estimate.

Errors due to a constant DC offset in the accelerometer signal are more severe since the same error is twice integrated. Integration of a step acceleration value results in a ramp in the velocity estimate, and integration of a velocity ramp affects the displacement estimate in a parabolic manner. In Figures Figure 2.1 through Figure 2.3, Ribeiro et al. (2002) show the effects of a DC offset equal to 0.0022 m/s^2 in the acceleration signal. This example shows how even a small offset in the accelerometer signal can produce severe errors in the velocity and displacement estimates.

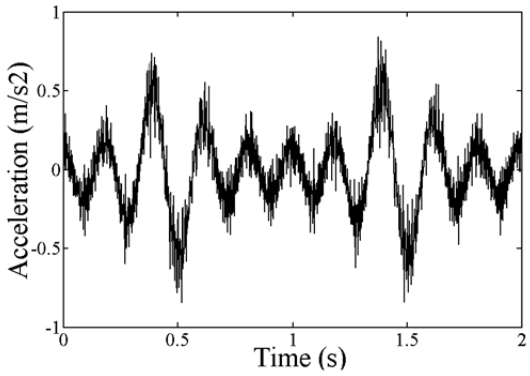

Figure 2.1 Piezoelectric accelerometer signal (Ribeiro et al., 2002)

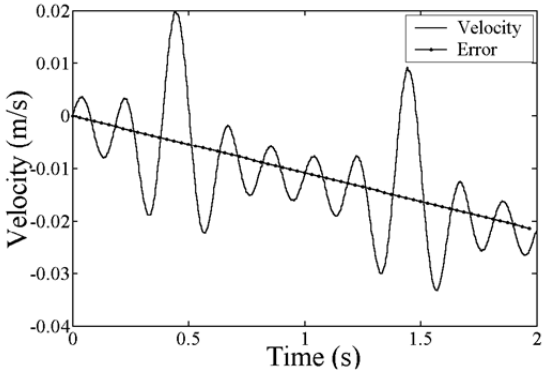

Figure 2.2 Estimated velocity with DC offset (Ribeiro et al., 2002)

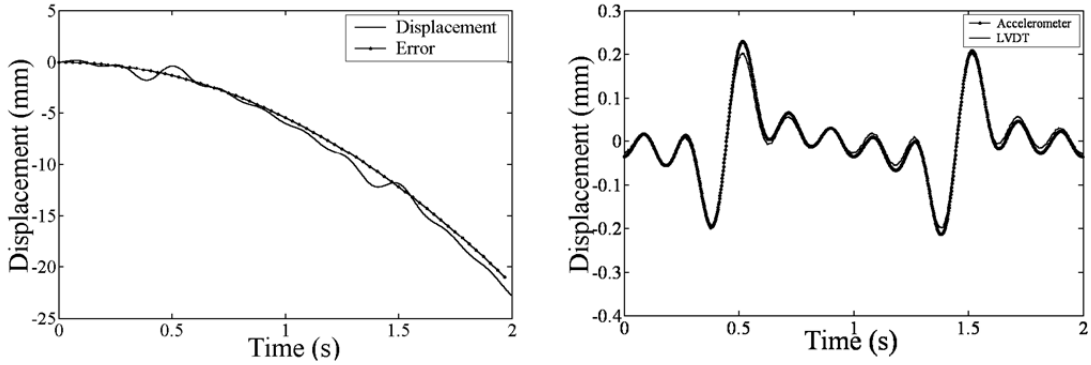

Figure 2.3 Estimated and actual displacements with DC offset (Ribeiro et al., 2002)

2.2.2 Conversion in the Frequency Domain

The Fourier transform can be used to convert a signal from the time domain to the frequency domain, and the inverse Fourier transform can convert the signal back to the time domain. Given a series of discretized acceleration data points, $[a_r]$, where $r = 0, 1, 2, \ldots, (N\text{-}1)$, and $t = r*\Delta t$, Han and Chung (2002) denote the discrete Fourier transform from definition as:

$$A_k = \frac{1}{N}\sum_{r=0}^{N-1} a_r e^{-i(2\pi kr/N)} \qquad k = 0,1,2,...,(N-1) \tag{2.6}$$

From the properties of the Fourier transform of the integral and double integral of Eq. 2.6, the researchers derive the following expressions for the Fourier transform of velocity and displacement, respectively:

$$V_k = \frac{1}{i2\pi k} A_k \qquad k = 0,1,2,...,(N-1) \tag{2.7}$$

$$D_k = -\frac{1}{(2\pi k)^2} A_k \qquad k = 0,1,2,...,(N-1) \tag{2.8}$$

The terms in the Fourier series are sorted by frequency in ascending order. It can be seen that displacement terms with very low k (low frequency components) will be magnified, while those with very high k (high frequency components) will be suppressed. The term for $k = 0$ represents a constant DC offset and can be zeroed before performing an inverse transform back into the time domain.

As technology improved over time, many commercial software packages developed algorithms to compute the fast Fourier transform (FFT), which gives the terms of the discrete Fourier transform with much higher computational efficiency. To obtain

the frequency spectrum of an acceleration signal with a sampling rate of 512 Hz and 8192 sampled points, Ribeiro et al. (1999) give a typical fft algorithm in MATLAB:

```
f = 512/8192 * [(0:1:4095)  (4096:-1:1)];
A = fft(a);
plot(f, abs(A));
```

Terms 2 through *N*/2-*1* in the FFT are symmetric with terms *N*/2+*1* through *N*. The first term is a constant DC offset, and term *N*/2 is the point of symmetry. Following the algorithm, the frequency vector in MATLAB corresponding to the first half of the FFT is:

$$f = [0, 1, 2, \ldots , f_s t/2] * f_s / (f_s t)$$

where

t: length of acceleration signal segment in seconds

f_s: sampling frequency

This reduces to:

$$f = [0/t, 1/t, 2/t, \ldots , f_s/2] \tag{2.9}$$

To convert from acceleration to displacement in the manner of Eq. 2.8, the FFT of acceleration (A = fft(a)) should be divided by $(2\pi f)^2$ so that:

$$D=\frac{A}{(2*pi*f)^2}$$

where each term in the displacement vector is:

$$D(k)=\frac{A(k)}{((k-1)/t)^2} \tag{2.10}$$

For very large *t*, the first few elements in Eq. 2.9 become very small. These elements correspond to the non-contributing low frequency components of the signal. Consequently, the vector elements in Eq. 2.10 are distorted in a parabolic manner after the conversion. This suggests that the conversion of acceleration to displacement in the frequency domain should be done for short segments of the acceleration history to avoid significant errors resulting from low-frequency noise.

2.3 SIGNAL PROCESSING IN EARTHQUAKE STUDIES

The most prevalent application of displacement estimation from accelerometer data is in the study of earthquakes. Boore et al. (2002) investigated the effects of different correction errors on the strong-motion data from the 1999 Hector Mine, California, earthquake in order to estimate ground velocity and displacements. Digital recordings of acceleration during earthquakes are practically guaranteed to have at least some baseline offset(s). Even small offsets can cause extreme errors in the velocity and displacement estimates upon integration, and these effects constitute the main challenge in the field of study. Boore explains that knowledge of the precise sources of errors would significantly improve the ability to apply universal correction methods, but in reality the errors are affected by many factors. One problem related to the instrument is accelerometer hysteresis, which is the lag of the sensor response to changes in forces. Another source of instrument error comes from static buildup in the analog-to-digital converter. The researchers also show that even a slight tilting of the ground during motion could produce an offset. A tilting of 0.06 degrees can produce a 1.3 cm/sec^2

offset in an acceleration signal whose peak amplitude is greater than 300 cm/sec^2, but the resulting displacement estimate after 50 seconds drifts all the way to a value of 10 m.

The most common solution is to apply a baseline correction. This process fits either a straight line or a polynomial to the portion of the velocity or displacement estimate that displays a drift, and then subtracts that curve from the data. A preliminary correction is almost always applied to the acceleration data, in which the mean of the pre-event acceleration trace is removed as a way of performing zero calibration on the results. The general procedure proposed by Boore (2001) is to fit a quadratic to the velocity estimate, remove the derivative of that quadratic from the acceleration, and then double integrate the corrected acceleration to obtain displacement. The key parameters in this method are the start and end times, t_1 and t_2 of the time segment on which the curve-fitting is applied. Although the researchers try to pick t_1 as close as possible to the start of the seismic event, they find that the displacement is highly sensitive to the parameters chosen. The type of drift can also vary among records, and the authors emphasize that the correction scheme must be fine-tuned intuitively for each separate case. On the other hand, the researchers find that the parametric results show very little variation for oscillation period less than 20 seconds. Since seismic analysis on structures is often limited to time periods within this limit, the researchers feel the results are nevertheless useful for earthquake engineering.

Chiu (2012) proposed a unique correction algorithm, in which he introduced a third order polynomial at the beginning of the acceleration signal. This polynomial, referred to as a "prefix acceleration impulse" by the author, is in the form of

$$I_a = et + ft^2 + gt^3 \tag{2.11}$$

where e, f, and g are unknown coefficients. Using known initial conditions a_o, v_o, and d_o for a value of t equal to the chosen length of the impulse, L (seconds), the coefficients can be determined. Chiu found that the calculated displacement signals exactly match the disseminated signals from national geological institutions. This result is significant, since strong compatibility between acceleration, velocity, and displacement is not often available. Nevertheless, compatibility is important in dynamic analyses of structures and soils, as well as the evaluation of Fourier and response spectra (Boore, 2005). The shortcoming of this algorithm in predicting displacements is that the initial conditions must be known. This can be overcome if the initial conditions are known to be zero, which is a reasonable expectation when an isolated force response is the subject of interest. Another problem is that the acceleration signal needs to be filtered and corrected for any offset or drift beforehand. In previous discussions, this correction is difficult to perform for arbitrary signals, where the sources of error and drift are unclear.

2.4 SIGNAL PROCESSING IN BRIDGE APPLICATIONS

The integration of acceleration signals in bridge applications poses different challenges from those in earthquake studies. Accelerometer drift is the main problem in strong-motion data, but low-frequency content is typically insignificant in seismic excitation (Faulkner et al., 1996). Furthermore, initial conditions are often known and equal to zero. Lastly, the forced displacement response in an earthquake is oscillatory. In bridge traffic applications, none of these conditions can be expected. Very low frequency components during forced vibration contribute to the low-frequency, pseudo-static response of the bridge. If these components are removed with filters, then the

displacement estimate becomes severely distorted. Faulkner found that the high-pass filter removal of 1Hz frequencies resulted in large errors on the forced vibration segment of the estimated displacement signal, while the free vibration segment was accurately predicted. Analysis of the frequency spectra of the forced vibration segment showed that a significant frequency component was present at 0.48Hz, while the frequency spectra of the free vibration segment did not show any significant frequency components less than 2-3Hz. This confirmed that the pseudo-static response comprises very low frequency components less than 1Hz. Faulkner found that high-pass filters were altogether unsuccessful, as no appropriate cutoff frequency could be found.

Faulkner et al. also performed a comparison of accelerometer parameters. They found that a force/balance accelerometer that detected frequencies down to 0Hz resulted in much better estimates of both the displacement waveform and spectra when compared to a high-sensitivity accelerometer with a range of 1Hz to 5000Hz. This again supported the concept that the low frequency components are of interest in determining the bridge response. The other parameter investigated was sampling rate. For a 400Hz sampling rate, the researchers were able to accurately predict the displacement signal when integrating the combined free and forced vibration segments of the acceleration history at once. For the 200Hz sampling frequency, the peak displacement estimates were highly inaccurate when the full acceleration record was integrated. When the isolated forced vibration segment was integrated, however, the results were significantly improved.

A study by Paultre et al. (1995) utilized a combination of accelerometers, strain gauges, and displacement transducers to model the dynamic response of existing bridges. The researchers were interested in evaluating the dynamic amplification of traffic loads

caused by bridge-vehicle dynamic interaction. These dynamic effects are related to the natural frequency of the bridge and are superimposed on the pseudo-static response. The purely pseudo-static response was isolated by applying a low-pass filter to remove frequencies greater than or equal to the natural frequency of the bridge. This was then compared to the unfiltered response in order to determine the dynamic amplification factors. The researchers also showed that accelerometer data could be integrated to approximate the displacement response, using a high-pass filter to remove low frequency noise and baseline correction to account for sensor drift. However, the authors provide no specific details regarding their correction methods.

Baseline correction was also used by Douglas et al. (1990) to integrate accelerometer data from quick-release experiments. These experiments were performed by applying a hydraulic load on an existing bridge to cause an initial deformation and subsequently quick-releasing the load. In the study, the load was applied transversely to the central pier. The displacements found by integrating the accelerograms compared well with LVDT measurements. However, this type of loading tends to cause bridges to vibrate at their natural frequencies, which are significantly higher than the pseudo-static response frequencies of normal truck traffic. Since the correction methods in the study do not account for low-frequency noise, the processing techniques are more suited for evaluating seismic loads rather than typical traffic loads.

Park et al. (2004) focused on correcting the displacement estimate drift resulting from non-zero initial velocity. Using a process referred to as the velocity estimation method, the researchers were able to accurately predict displacement by double integrating acceleration. The procedure essentially consists of the double integration of

acceleration to produce a displacement estimate. This displacement is then differentiated to obtain a velocity estimate. The mean of this velocity trace, is not equal to zero, is used as an estimate of initial velocity for a subsequent iteration to obtain a new displacement estimate. Iteration is performed until the average of the derivative of displacement is equal to zero. The procedure does not require any filtering or baseline correction, but the removal of the mean offset of acceleration is still required. Furthermore, the initial displacement must be known. This is reasonable for isolated forced vibration events. Furthermore, high-pass filters would be the only alternative method for overcoming unknown initial conditions, but such filters cannot be used due to the contribution of the low-frequency, pseudo-static response.

Following Faulkner's recommendations, Gindy et al. (2007) performed integration on the isolated free and forced vibration segments of the acceleration record in order to predict velocity and displacement. The researchers improved the accuracy of the results by performing baseline correction on the velocity trace before a second integration to obtain displacement. They also refined the method by which the forced vibration segment is distinguished from the free vibration segment. Use is made of the Arias Intensity (I_A), given by:

$$I_A = \int a^2(t)dt \tag{2.12}$$

The Arias Intensity is typically used in seismic analysis to quantify the intensity of seismic forces. Gindy et al. use Eq. 2.12 on the entire acceleration record to determine the boundaries of the forced vibration segment. Times t_1 and t_2 were selected as the locations of the 5th and 95th energy levels (Figure 2.4).

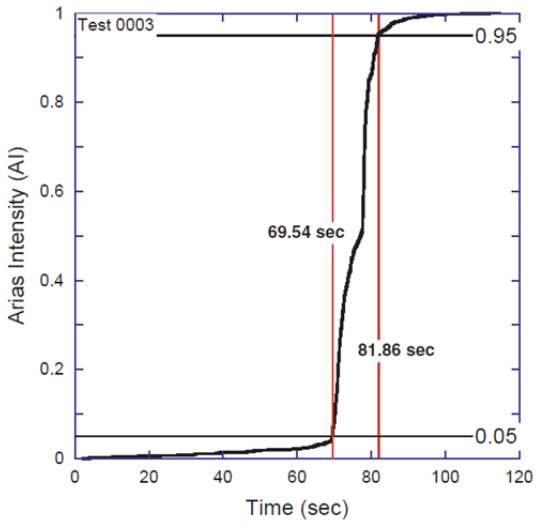

Figure 2.4 I_A plot for forced vibration boundary selection (Gindy et al., 2007)

Lastly, the researchers compared the displacement estimates with those obtained using the velocity estimation method by Park et al. (2004). Gindy et al. find that the knowledge of initial velocity does not significantly improve the accuracy of the displacement estimate when initial conditions are nearly zero. Instead, the correction of the accelerometer drift using baseline correction after the first integration will have a larger impact. Combined with the isolation of the free and forced response segments, the maximum displacements were accurately estimated.

CHAPTER 3

FIELD TESTING PROGRAM

3.1 INTRODUCTION

The objective of the field testing program was to measure the structural response of the NJTA Interchange 7A Bridge (Structure No. 60.51I) and the Hackensack River Bridge (Structure No. E109.83) due to large live loads. Acceleration, velocity, displacement, and strain were measured directly using various instruments. The field results allowed for a wide range of analyses and signal processing operations, so that a comprehensive investigation could be made on the full response spectra of the bridges.

3.2 EQUIPMENT

The instruments used in the field include accelerometers, strain transducers, and a Laser Doppler Vibrometer (LDV). Two separate data acquisition systems are used: the Structural Testing System and the SoMat eDaq.

3.2.1 Structural Testing System (STS)

The STS system, manufactured by Bridge Diagnostics Inc. (BDI), is used for data acquisition of the accelerometer and strain transducer readings. The components of the system are modular. The sensors are cable-connected directly to junction boxes (Figure 3.1), which then transmit the data wirelessly to a single base station from distances of up

to 200 feet. Each junction box contains four channels, and a total of 400 channels are available for the entire system. A microchip and unique identification number for each sensor and junction box allows for automatic identification within the system, such that the sensors can be identified without knowledge of the channel connections. Thus, a major advantage of the system is that an arbitrary wiring scheme can be used at any time, and sensors moved within the system are automatically tracked and identified. The STS can be controlled with a notebook computer via a Wi-Fi internet connection. BDI provides its own dynamic analysis software to control sampling rate, test duration, file names, and zero calibration, while calibration factors are automatically applied from stored files in the software package.

Figure 3.1 Structural Testing System (STS). From left to right are the base station, junction box, and transducer.

3.2.2 BDI Accelerometers

The accelerometers are used with the STS system. These capacitive sensors can measure accelerations in the range of ±5g (49,050 mm/s^2) for frequencies of 0-400Hz. On structural steel members, the sensor can be attached using clamps or bolts and removed after use. To measure rebar vibrations, the sensors can be zip-tied to rebars, as

shown in Figure 3.2, and removed after use or otherwise embedded in concrete for permanent installation. The instruments detect accelerations in the axis perpendicular to its broad face, which is the face shown in Figure 3.2. As such, they must be securely attached to prevent tilting and rotation.

Figure 3.2 BDI capacitive accelerometer

3.2.3 BDI Strain Transducers

Strain transducers were also used in the STS system. They are installed in a similar manner as the accelerometers in that they can either be clamped or bolted in place (Figure 3.3). The sensor has a rugged and waterproof aluminum frame approximately 4 inches long. It is sensitive to noise and therefore utilizes a 5-conductor shielded cable. The instrument can measure strains in the range of ±2000με along its longitudinal axis.

Figure 3.3 BDI strain transducer

3.2.4 Laser Doppler Vibrometer

The Laser Doppler Vibrometer (LDV) is used to measure displacement and velocity of a point at a distance of up to 600 feet. Manufactured by Polytec PI, the LDV uses laser interferometry. Motion of the target point relative to the laser head produces a Doppler shift in the light frequency that can then be converted into displacement and velocity. Application of the device at long ranges will often require the use of reflective tape at the point of interest in order to improve the signal (Figure 3.4). For maximum signal strength, the LDV should also be aimed directly perpendicular to the target surface. To measure bridge girder deflection, for example, the users must carefully position the LDV directly underneath the target location on the girder. This is assuming that the girder bottom flange is horizontally level, which is typically the case. The laser head, which is of helium neon Class II, is mounted on a tripod that must be relocated in order to monitor different targets. Relocation takes approximately 10-15 minutes in order to obtain adequate signal strength. The delicate nature of the system relegates its use to short tests under fair weather conditions.

Figure 3.4 Polytec PI Laser Doppler Vibrometer (LDV) underneath the Hackensack River Bridge

3.2.5 SoMat eDaq

The SoMat eDaq is a portable data acquisition system used in this study exclusively to control the LDV. The system has two separate channels for receiving and decoding displacement and velocity data from the LDV. As such, the two quantities are saved in separate files for displacement and velocity. Both the LDV and eDaq require an external power source, such as 12V vehicular power. Consequently, the applicability of these systems to measure bridge deflection is highly dependent on the accessibility beneath the bridge.

3.3 INSTRUMENTATION OF NJTA INTERCHANGE 7A BRIDGE (STRUCTURE NO. 60.51I)

The bridge, which shall be referred to as the 7A Bridge, is a two-span continuous steel curved bridge with a system of composite girders and diaphragms (Figure 3.5 and Figure 3.6). A transverse steel box girder is used to transfer the load to the intermediate

support, giving two similar 150 ft. spans. Located at milepost 62 on the New Jersey Turnpike, the structure was incomplete at the time of the field testing, as it is a part of a series of new bridges that comprise the 7A interchange.

Figure 3.5 Overview of the 7A Bridge (facing south)

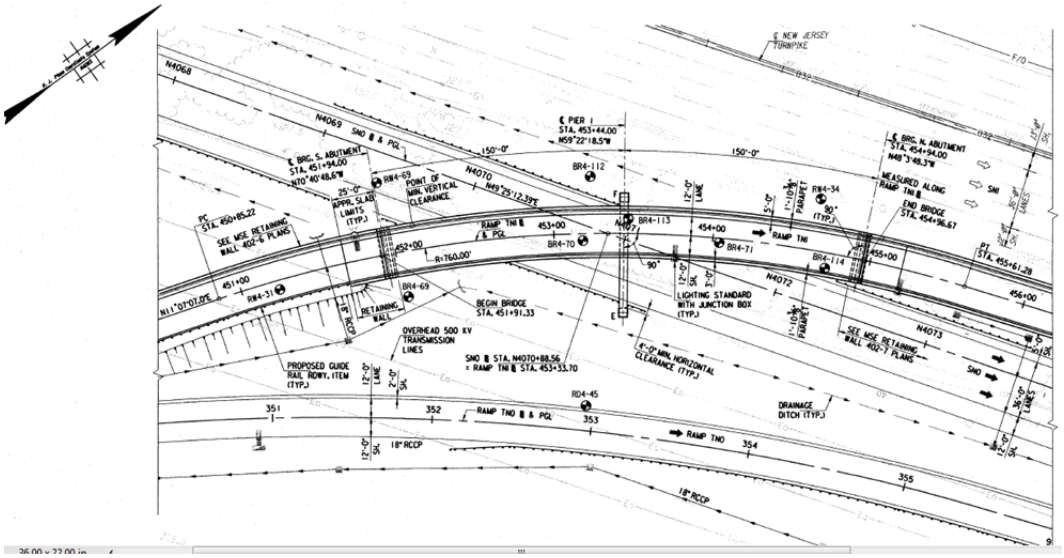

Figure 3.6 Structural plan of 7A Bridge

3.3.1 Instrumentation

On September 20, 2012, researchers from Rutgers University instrumented the 7A Bridge. The sensor locations can be seen in Figure 3.7. Sensors S1 through S16 are strain transducers installed on the bottom of the girder bottom flanges. Sensors A1 through A4 are accelerometers also installed on the bottom of the girder bottom flanges, except for A3 which is installed on the side of the east side of the Girder 3. The names D1 through D10 correspond to LDV measurement points on the girder bottom flanges, where reflective tape was attached. Only one location was monitored by the LDV per test.

The locations instrumented were the quarter spans and the box girder at the support. Since the bridge is continuous, the maximum deflection does not occur exactly at a midspan. However, the quarter span and midspan locations corresponded to diaphragm locations. This provided simple reference locations and eliminated the need for long distance measurement of the final sensor locations. The researchers were also aware of the stress concentrations very close to the diaphragms, so all sensors shown in Spans 1 and 2 were actually installed 2 feet north of the quarter span and midspan locations.

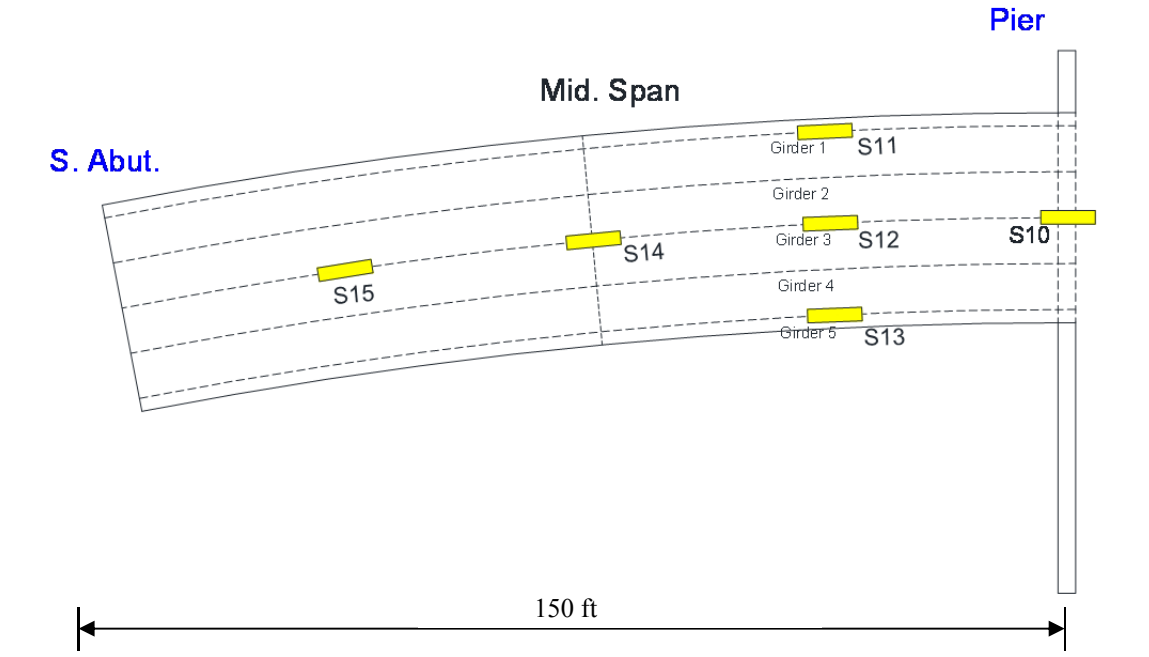

(a)

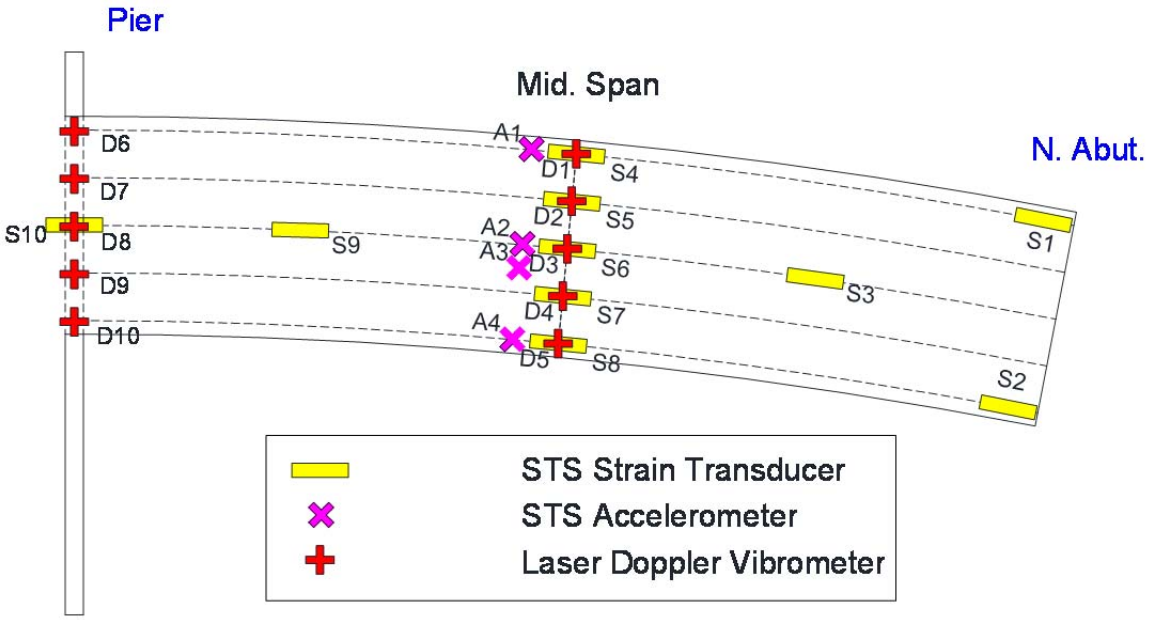

(b)

Figure 3.7 Instrumentation plan: (a) Span 2, (b) Span 1

3.3.2 Testing Procedure

The main approach in the field testing was to subject the bridge to live loading from a single truck at different speeds. This would provide a comprehensive evaluation of the bridge structural response for finite element model (FEM) calibration and signal processing. Although the FE analysis is not included in this study, the data collected in the field tests were sufficient for model calibration. The testing parameters were the vehicle speed and the LDV location. The calibration truck had a total weight of 56.68 kips with the axle configuration shown in Figure 3.8. Guiding cones were placed along the bridge so that the truck could only travel in a designated lane at a measured transverse location on the deck. This allowed for excellent consistency and was necessary for modeling load cases in FE analysis. The truck traveled from north to south in each test. The details of the individual tests are given in Table 3.1.

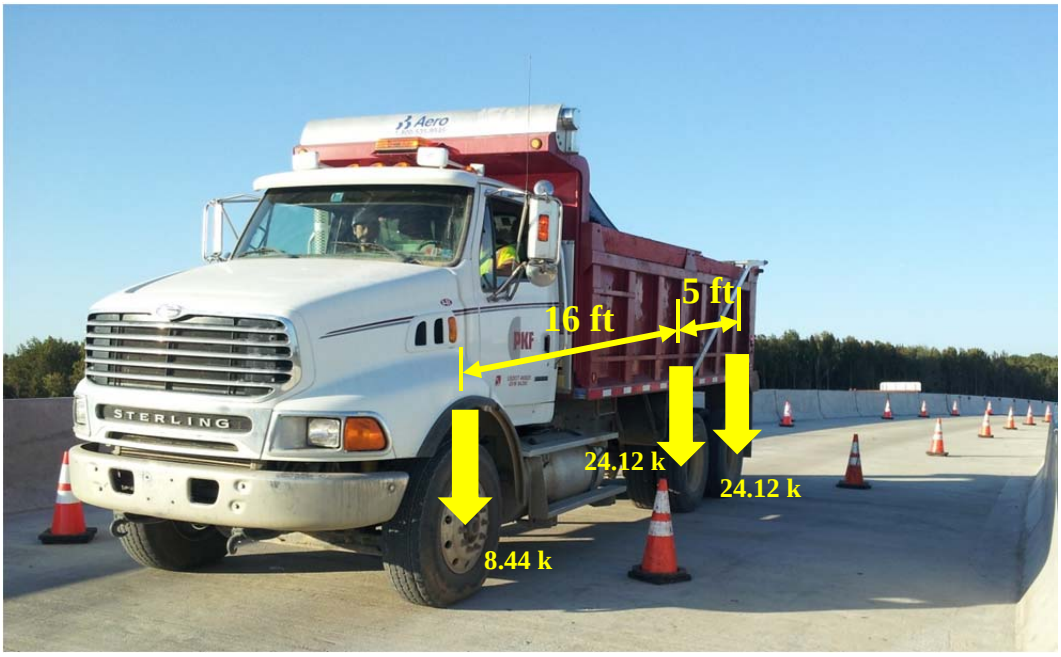

Figure 3.8 7A Bridge calibration truck

Table 3.1 Summary of 7A Bridge field test parameters

Test No.	Test name	LDV placement		Speed (mph)
		Span	Girder	
1	G1_1	1	1	5
2	G1_2	1	1	5
3	G1_3	1	1	20
4	G1_4	1	1	20
5	G1_5	1	1	40
6	G1_6	1	1	40
7	G2_1	1	2	5
8	G2_2	1	2	5
9	G2_3	1	2	20
10	G2_4	1	2	20
11	G2_5	1	2	40
12	G2_6	1	2	40
13	G3_1	1	3	5
14	G3_2	1	3	5
15	G3_4	1	3	20
16	G3_7	1	3	20
17	G3_3	1	3	25
18	G3_5	1	3	40
19	G3_6	1	3	40
20	G4_1	1	4	5
21	G4_2	1	4	5
22	G4_3	1	4	20
23	G4_4	1	4	20
24	G4_5	1	4	40
25	G4_6	1	4	40
26	Girder5_1	1	5	5
27	Girder5_2	1	5	20
28	Girder5_3	1	5	40

For signal processing, the tests of interest are those with truck velocities of at least 20 mph, because they result in shorter integration periods. Also, there are no acceleration data available for Girders 2 and 4. This reduces the number of runs that meet the criteria for analysis. On the other hand, all tests, regardless of LDV location, contain acceleration data for Girders 1, 3, and 5. To increase the number of available tests for analysis, Girder 3 acceleration data are used from tests G1_5, G1_6, and G5_3.

Displacement estimates from these accelerations are then compared with LDV results from test G3_6. Since the bridge response on Girder 3 was consistent for all tests of the same speed, these comparisons are still valid. Given these additional tests, a healthier sample size of 13 tests were available for error analysis.

The general procedure for any particular test starts with the LDV placement and adjustment. For large distances between the laser head and the target point, the signal strength must be checked before each test. Because the tripod is often placed on uneven ground, the LDV tends to move slightly due to ground vibrations. Therefore, small adjustments of the angle and focus are often necessary to strengthen the signal. After finalizing the laser settings, all instruments are zeroed before beginning the test. Next, the truck driver or observer on the deck will communicate to the test conductors when to start and end the test. Tests are initiated and stopped using manual triggers in the system software. The software dynamically displays the result, and the test is concluded with a quick verification of the graphical results.

The results that are immediately available in the field are measured acceleration, velocity, displacement, and strain. Typical results for Girders 1 and 3 with truck speeds of 40 mph are shown in Figure 3.9 and Figure 3.10. A sampling rate of 100 Hz was used for all instruments across all tests. A challenge in this study was the proper synchronization of the two data acquisition systems, STS and SoMat eDaq, since the test initiation triggers are completely independent. When comparing results of the two systems, the time offset must be determined by visually comparing the STS strain results with the LDV displacement results, for which the start and end times of the isolated force response are often easy to deduce.

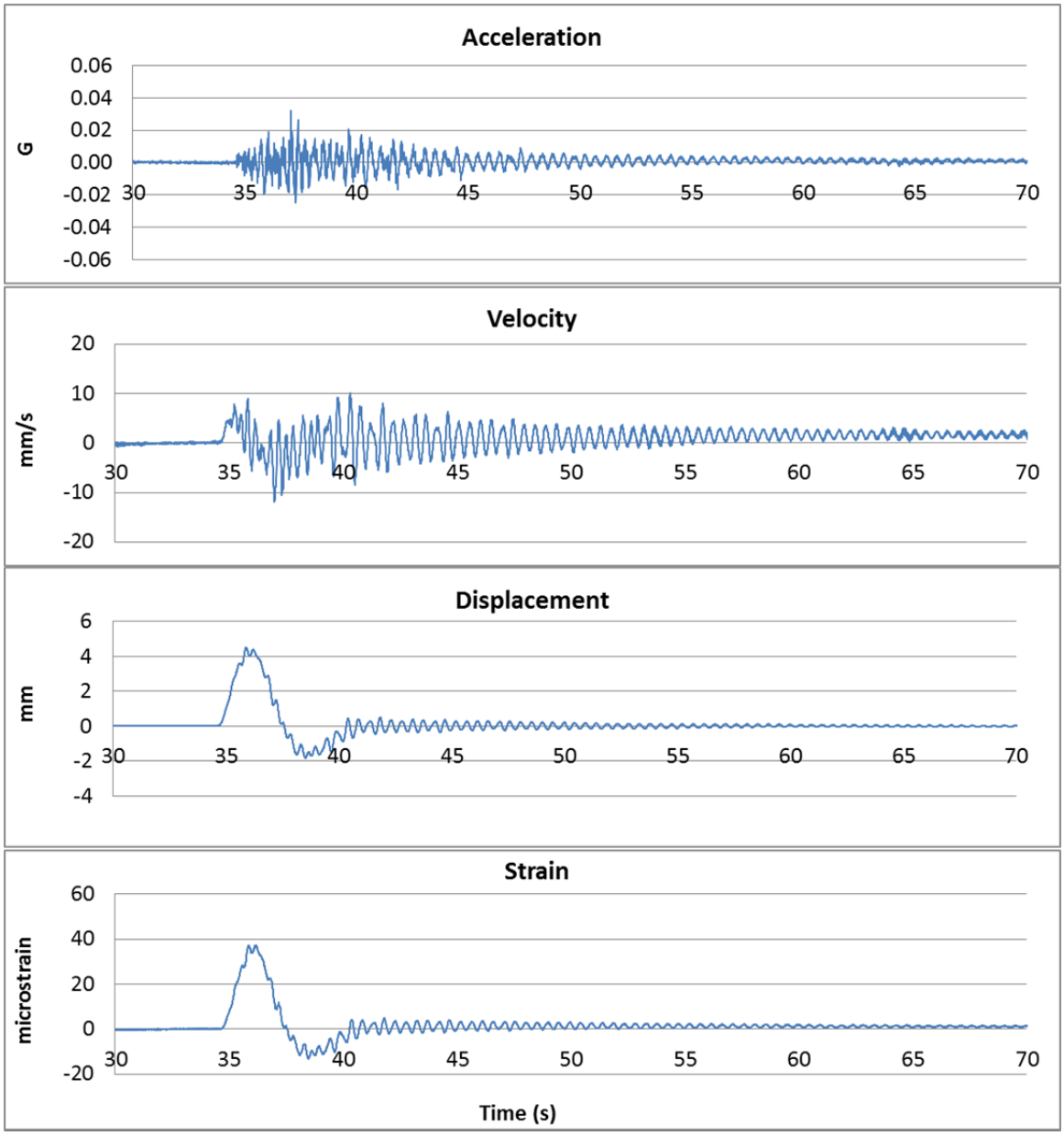

Figure 3.9 Bridge response for Test G1_6

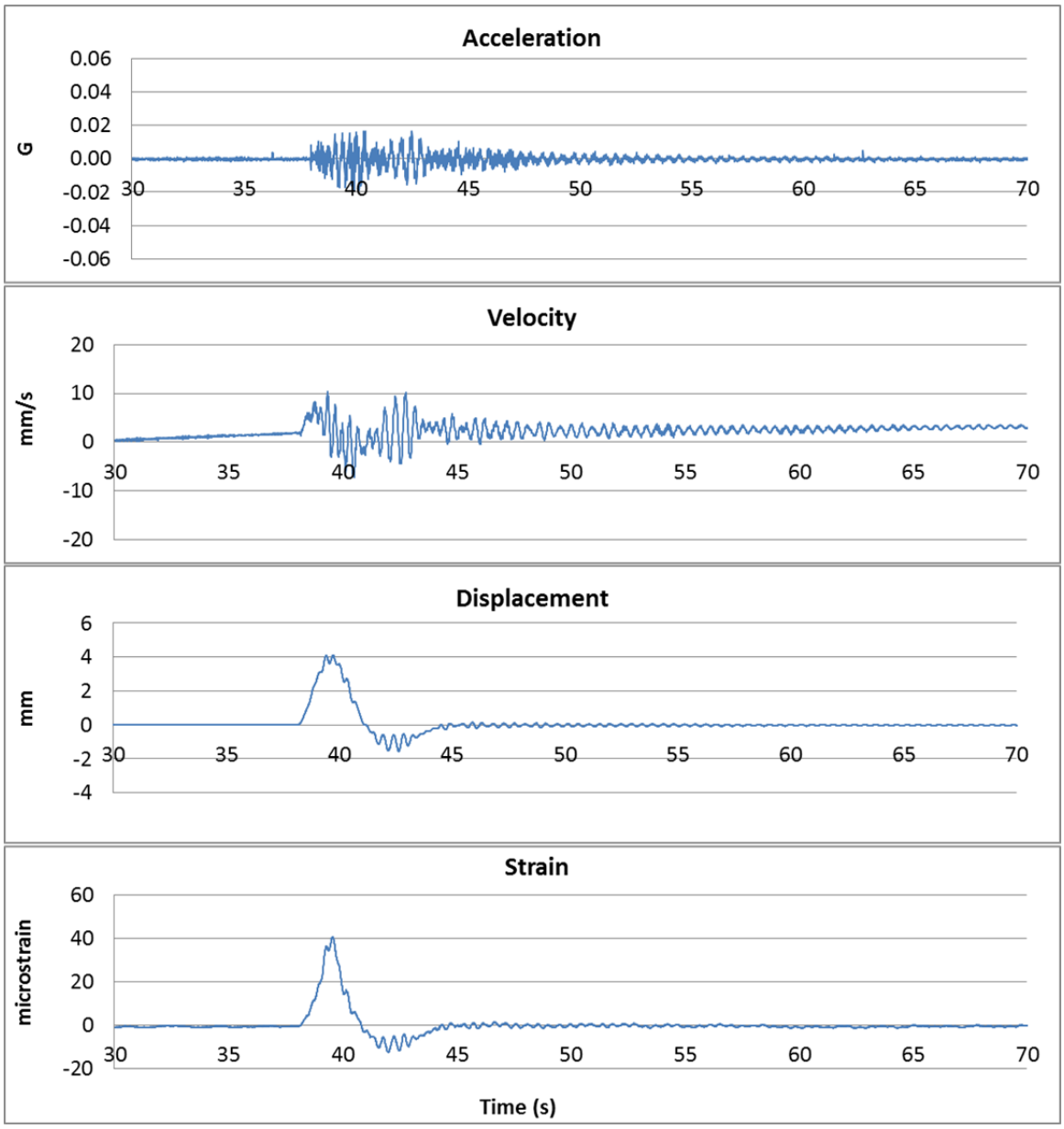

Figure 3.10 Bridge response for Test G3_5

The velocities show a small offset and drift from the zero position. A constant offset can be effectively corrected by removing the mean from the data. For a drift, the slope is determined so that a baseline can be removed from the data. These are typical data processing tasks that must be performed for most tests.

3.4 INSTRUMENTATION OF THE HACKENSACK RIVER BRIDGE

The Hackensack River Bridge is a 38-span bridge crossing the Hackensack River in New Jersey. It is located on the NJ Turnpike between Exits 15W and 15X. Originally completed in 1953, it underwent widening in the 1970s. The bridge elevation is shown in Figure 3.11. The main span is 375 feet, and the total length of the bridge is 5613 feet. It contains two types of span: floor beam spans and main truss spans. Typical floor beam spans are shown in Figure 3.12. This study focuses on Span N5, which is a simply supported floor beam span between Piers N5 and N6.

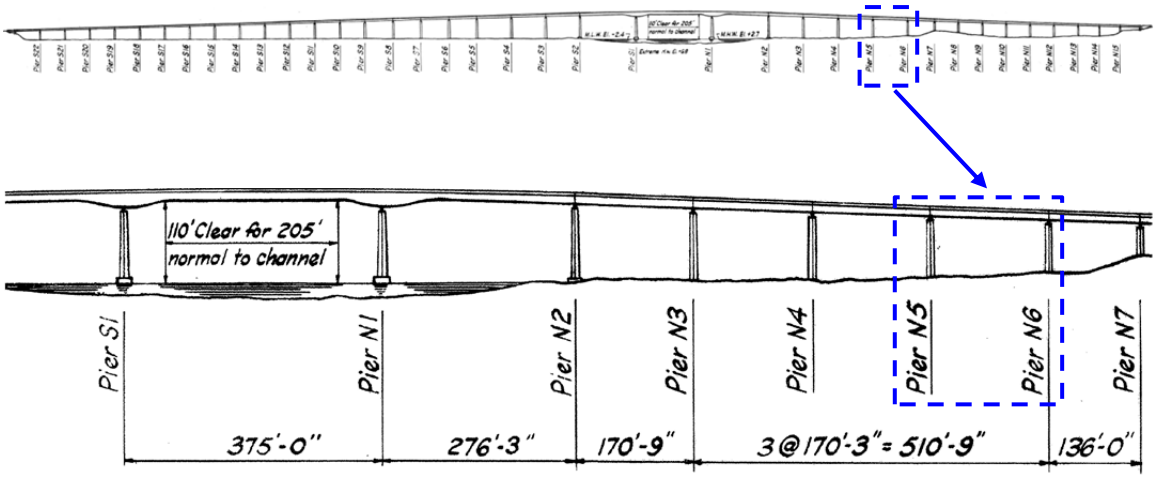

Figure 3.11 Hackensack River Bridge Elevation

Figure 3.12 Typical floor beam spans

The motivation for this study was the staged deck rehabilitation on the bridge, which exposed freshly placed concrete to live load effects from adjacent lanes. The construction is still in progress, and it is being performed without closing lanes or stopping traffic. For the project stage at the time of this study, the new deck for the median portion of the roadway was under construction for Spans N5 and N6. The lane configuration at that time is shown along with the future lane configuration in Figure 3.13.

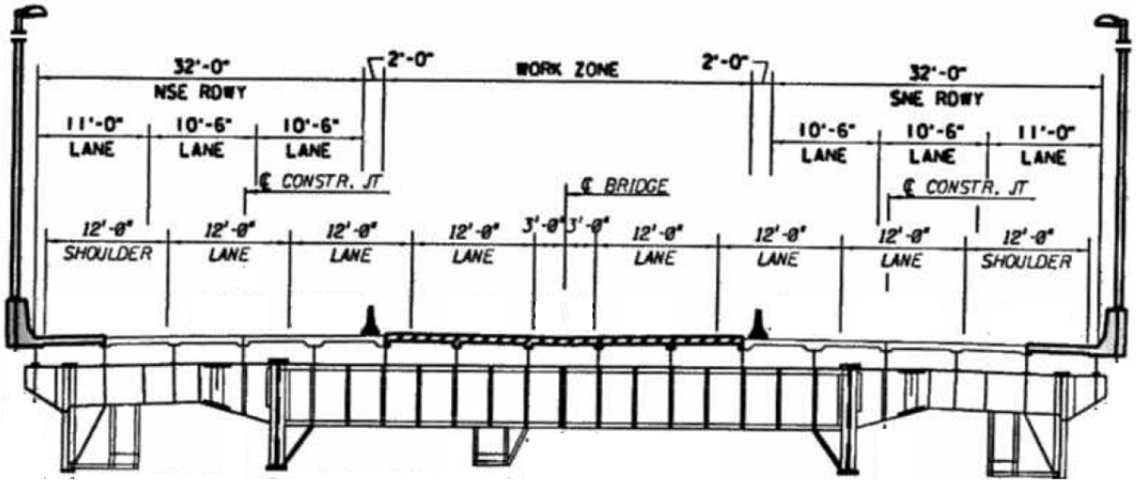

Figure 3.13 Section view of Span N5 under rehabilitation

3.4.1 Instrumentation

Instrumentation and field testing of the Hackensack River Bridge was performed by researchers from Rutgers University from July 25-27, 2012. One objective was to conduct preliminary tests to compare rebar vibrations for two different cases. The first case was for the condition of 50 percent tiedowns of the top mat of reinforcement, in which every other rebar intersection was tied. The second case was for the full tiedown condition in which every intersection was tied. These two cases are shown in Figure 3.14.

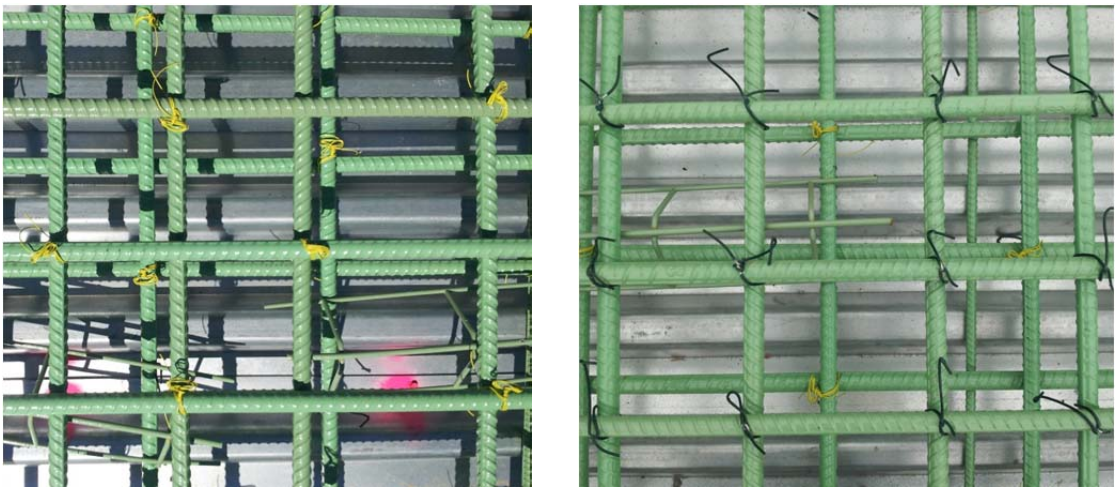

(a) (b)

Figure 3.14 Comparison of (a) 50% tiedowns, and (b) 100% tiedowns

The sensors for the primary testing program were installed on the second day, and the primary testing program was executed on the third and final day during the concrete pours on Spans N5 and N6. Only Span N5 was instrumented, and the sensor locations are shown in Figure 3.15 and Figure 3.16. Sensors S1 through S8 are strain transducers attached beneath the bottom flange of the girders. Sensors A1 through A5 were installed in a similar manner, except that A3 was installed on the flange of Floor Beam 5. The

labels R1 through R5 correspond to the target locations of the LDV on the bottom of the girder and floor beam bottom flanges, where reflective tape was attached. It was difficult to establish the LDV at ground level beneath the locations of R3 through R5, so the majority of LDV results are only for R1 and R2 on the WN5 girder and West Girder, respectively. Additionally, a significant amount of water was dripping from the bridge during the concrete pour and curing, making it impossible to place the laser on R2. As a result, the analysis of velocities and displacements during the pour is limited to R1 on the WN5 girder.

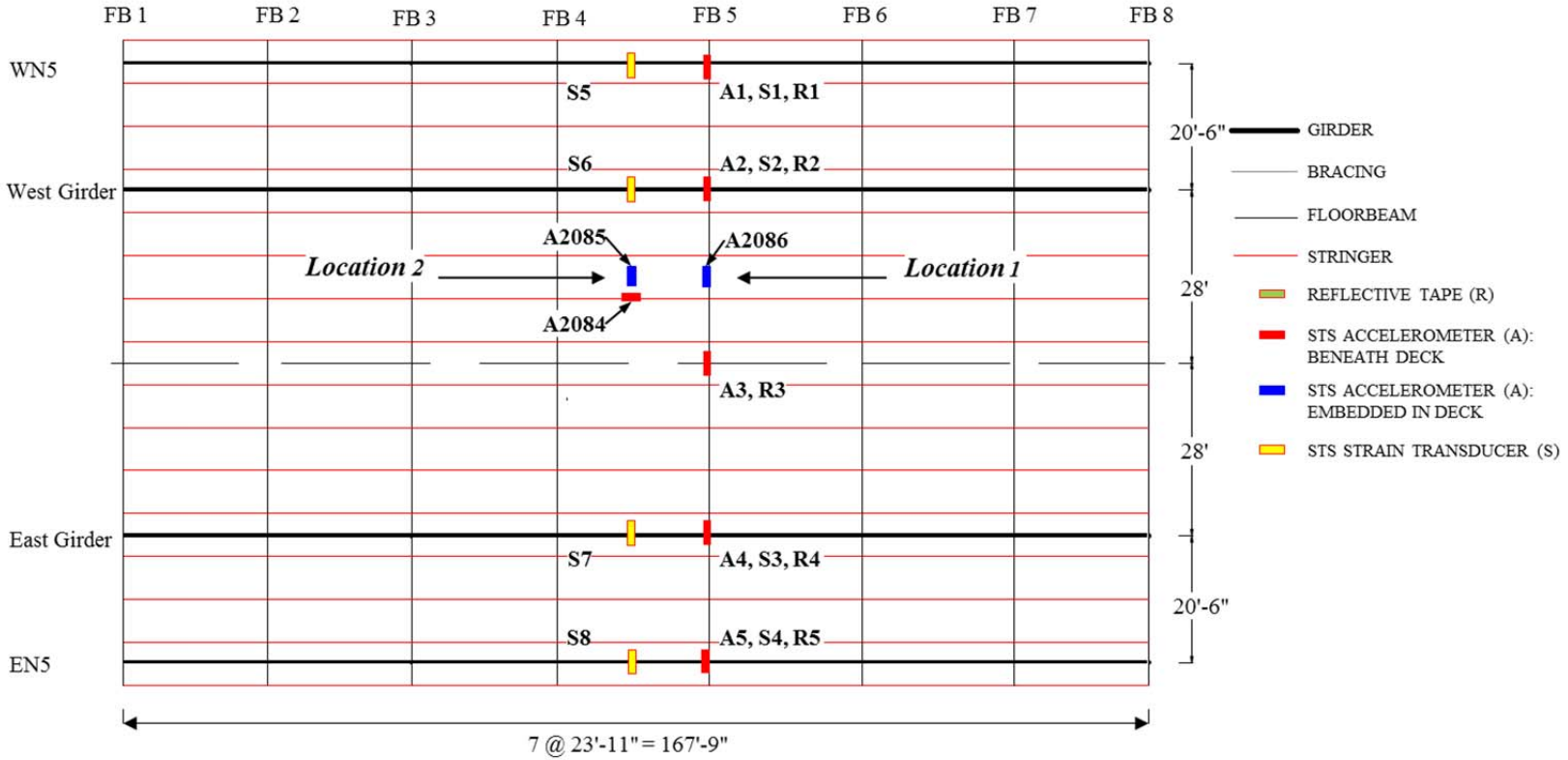

Figure 3.15 Instrumentation plan of Span N5

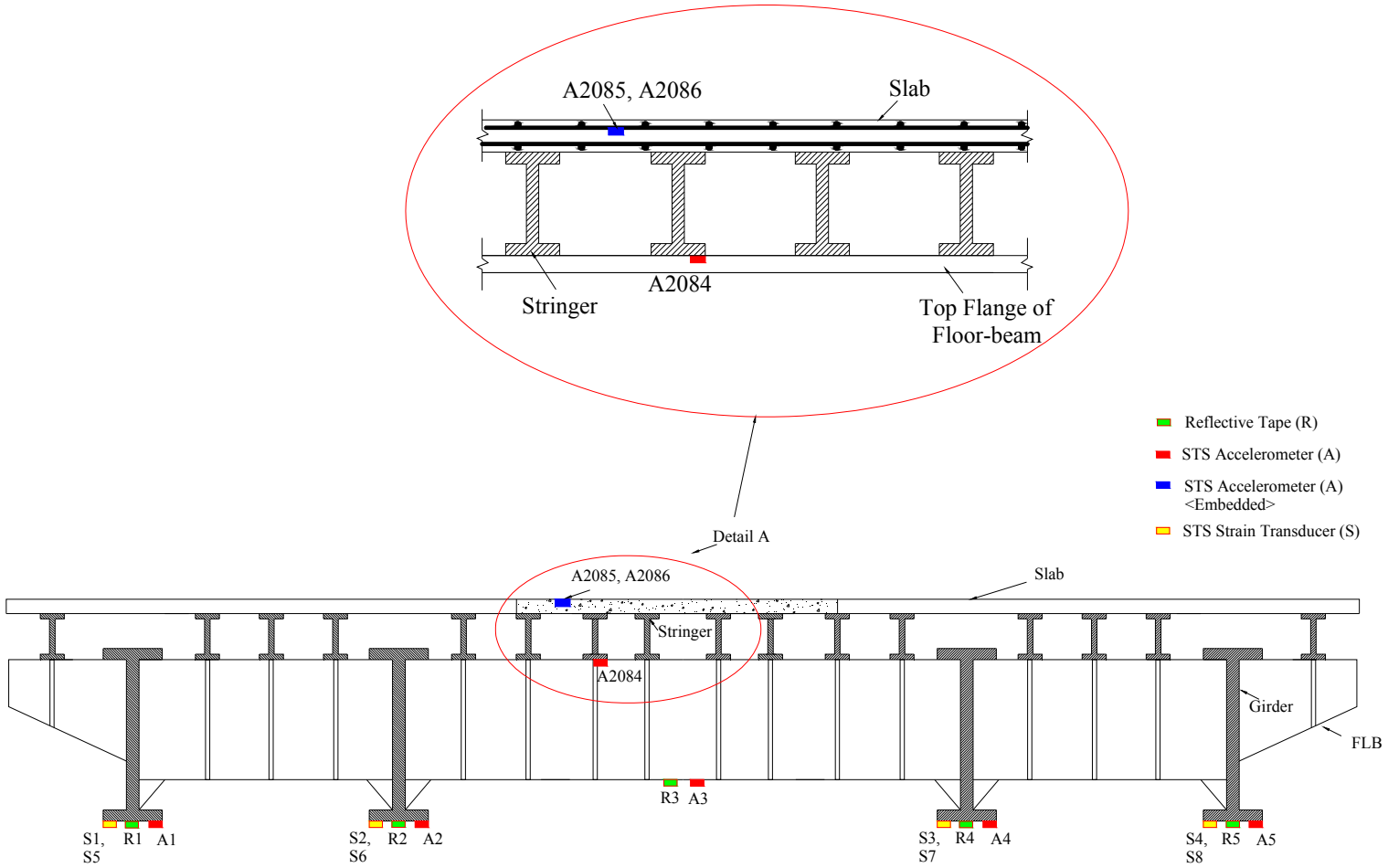

Figure 3.16 Section view of sensor locations between Floor Beams 4 and 5

Sensor A2084 was attached to the bottom flange of Stringer 7 (numbered from west to east). At nearly the same location on the deck (within 3 feet), Sensor A2085 was attached to a top mat rebar before the pour so that it would be permanently embedded in the deck. These two sensors (A2084 and A2085) were used to evaluate the motion of the top rebar relative to the formed metal deck and the surrounding deck concrete. Since the formed metal deck and concrete should exhibit very little motion relative to the stringer, a comparison of A2084 and A2085 signals provides a reliable method of evaluating of the rebar vibration within fresh concrete. A similar approach was taken to compare the rebar motion to the floor beam motion using Sensors A2086 and A3, but the transverse distance between these locations is much greater (approximately 10 feet). Therefore, the analysis of rebar debonding was primarily based on the A2084 and A2085 sensors.

3.4.2 Preliminary Test: Comparison of 50% and 100% Tiedowns

The preliminary test in this study was done to compare the tiedown conditions at two different locations. A sampling rate of 100 Hz was used for all tests. Location 1 is on top of Floor Beam 5, and Location 2 is midway between Floor Beams 4 and 5 (Figure 3.15). On the first day of testing, the top reinforcement layer was tied down at only 50 percent, that is, every other rebar intersection was tied down. During the peak traffic hours, accelerations data were collected for the top and bottom layer rebars at Locations 1 and 2. Since the bottom reinforcement mat is always fully tied down, the bottom rebar at each location was used as the reference point to evaluate the top rebar vibration. The second phase of the test was to return when 100 percent tiedowns were completed and collect additional data at the exact same rebar locations. Though the traffic live loads were expected to vary from day to day, these tests provided a basis of comparison.

The acceleration records for Locations 1 and 2 can be seen in Figure 3.17 and Figure 3.18. In all cases, the top layer rebar accelerations are noticeably larger than those of the bottom layer rebar. The most illustrative approach in comparing the tiedowns is to observe the isolated peaks or spikes in the acceleration record. At the 224 second mark, for example, a large spike of 0.547g can be observed in the top rebar at Location 1 with 50 percent tiedown. The corresponding spike in the bottom rebar layer is only 0.161g. A useful means of comparison is to compute the ratio of bottom rebar acceleration to top rebar acceleration. Values of this ratio close to 1.0 represent an effective tiedown case, where the top rebar motion is sufficiently constrained and is very close to that of bottom rebar. Values approaching 0 represent deficient constraints on the top rebar motion, such that the bottom rebar acceleration is much lower.

By sampling several acceleration peaks from each record, a numerical analysis can be made. Table 3.2 and Table 3.3 summarize the sampled peak accelerations at Locations 1 and 2, respectively. At Location 1, the average peak acceleration of the top rebar was 58% higher in the partial tiedown case than in the full tiedown case. At Location 2, the difference is less significant; the top rebar accelerations decreased by only 9.2 percent after full tiedowns were completed. Among the entire test data, the maximum acceleration observed for the top layer rebar was 0.547g with 50 percent tiedowns and 0.328g with 100 percent tiedown.

Table 3.2 Location 1 peak rebar accelerations

Location 1					
50% Tiedown			100% Tiedown		
Top Rebar Acceleration (G)	Bottom Rebar Acceleration (G)	Bottom to Top Ratio	Top Rebar Acceleration (G)	Bottom Rebar Acceleration (G)	Bottom to Top Ratio
0.334	0.203	0.608	0.276	0.220	0.797
0.257	0.051	0.198	0.161	0.086	0.290
0.221	0.053	0.230	0.152	0.097	0.643
0.295	0.110	0.372	0.253	0.133	0.525
0.547	0.161	0.295	0.126	0.094	0.749
0.178	0.092	0.519	0.207	0.110	0.531
Avg: 0.305	Avg.: 0.112	0.366	Avg: 0.193	Avg: 0.126	0.652

Table 3.3 Location 2 peak rebar accelerations

Location 2					
50% Tiedown			100% Tiedown		
Top Rebar Acceleration (G)	Bottom Rebar Acceleration (G)	Bottom to Top Ratio	Top Rebar Acceleration (G)	Bottom Rebar Acceleration (G)	Bottom to Top Ratio
0.250	0.181	0.725	0.178	0.173	0.970
0.096	0.056	0.580	0.210	0.180	0.850
0.181	0.081	0.451	0.179	0.153	0.850
0.278	0.145	0.522	0.180	0.163	0.900
0.278	0.181	0.649	0.282	0.237	0.840
0.336	0.183	0.545	0.328	0.288	0.870
0.216	0.131	0.606	0.153	0.130	0.840
Avg: 0.236	Avg.: 0.138	0.583	Avg: 0.215	Avg: 0.189	0.870

Although the tests were conducted during peak traffic hours, the traffic loads may have been too erratic to provide representative average accelerations for analysis. For a more reliable comparison, the ratios of accelerations for bottom to top rebars were compared for each tiedown case from Tables 1 and 2. In this comparison, a more pronounced change in the motion of the rebar system can be observed. With 50 percent tiedowns at Location 1, the ratio of accelerations for the bottom rebar versus the top rebar was 0.366, but this proportion increased to 0.652 in the full tiedown case. Similarly, the

50 percent tiedown at Location 2 resulted in a bottom to top ratio of 0.583, while the proportion was 0.870 for the full tiedown case. This demonstrates a significant reduction in vibrations of the top layer rebars.

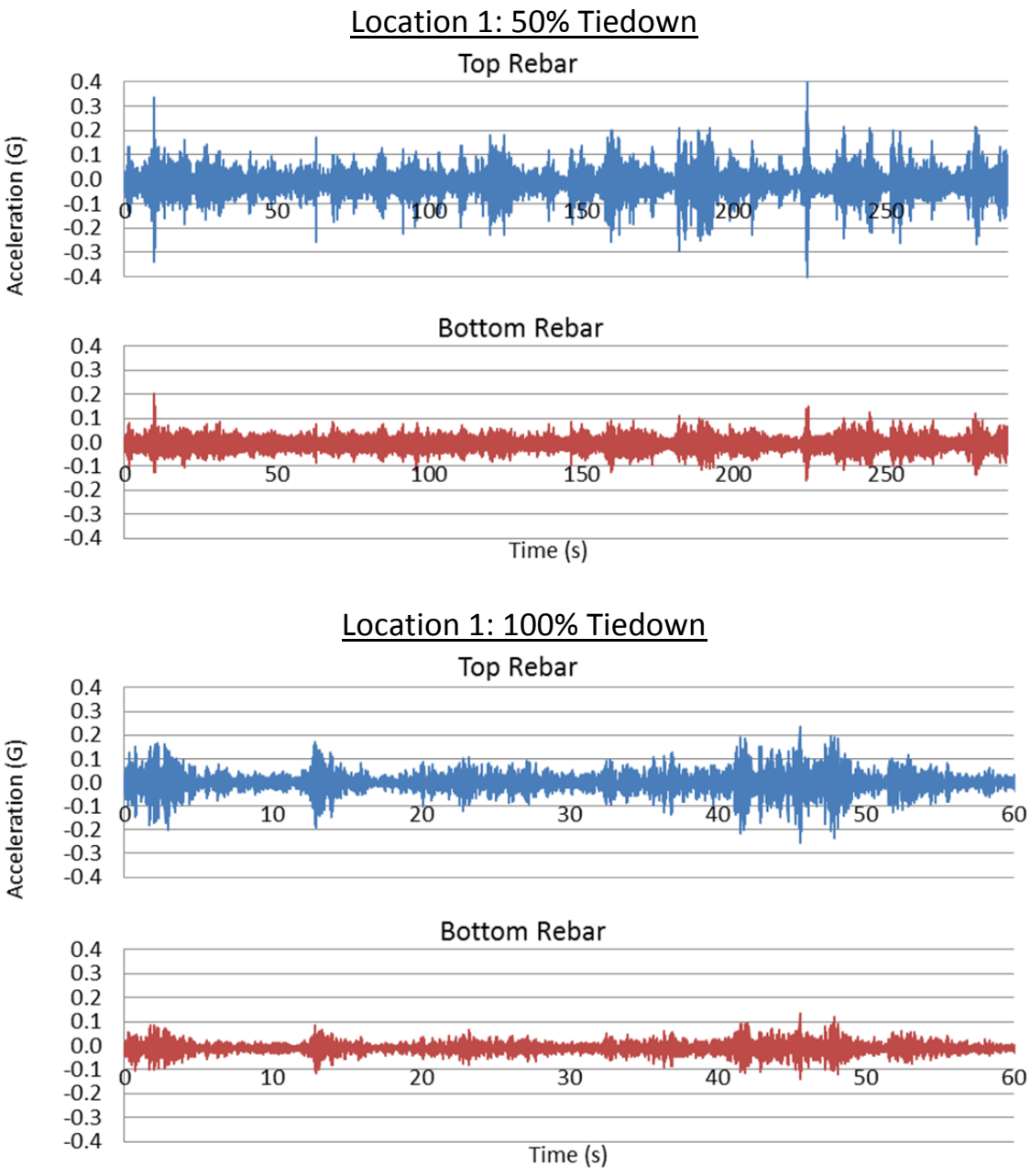

Figure 3.17 Location 1 tiedown comparison

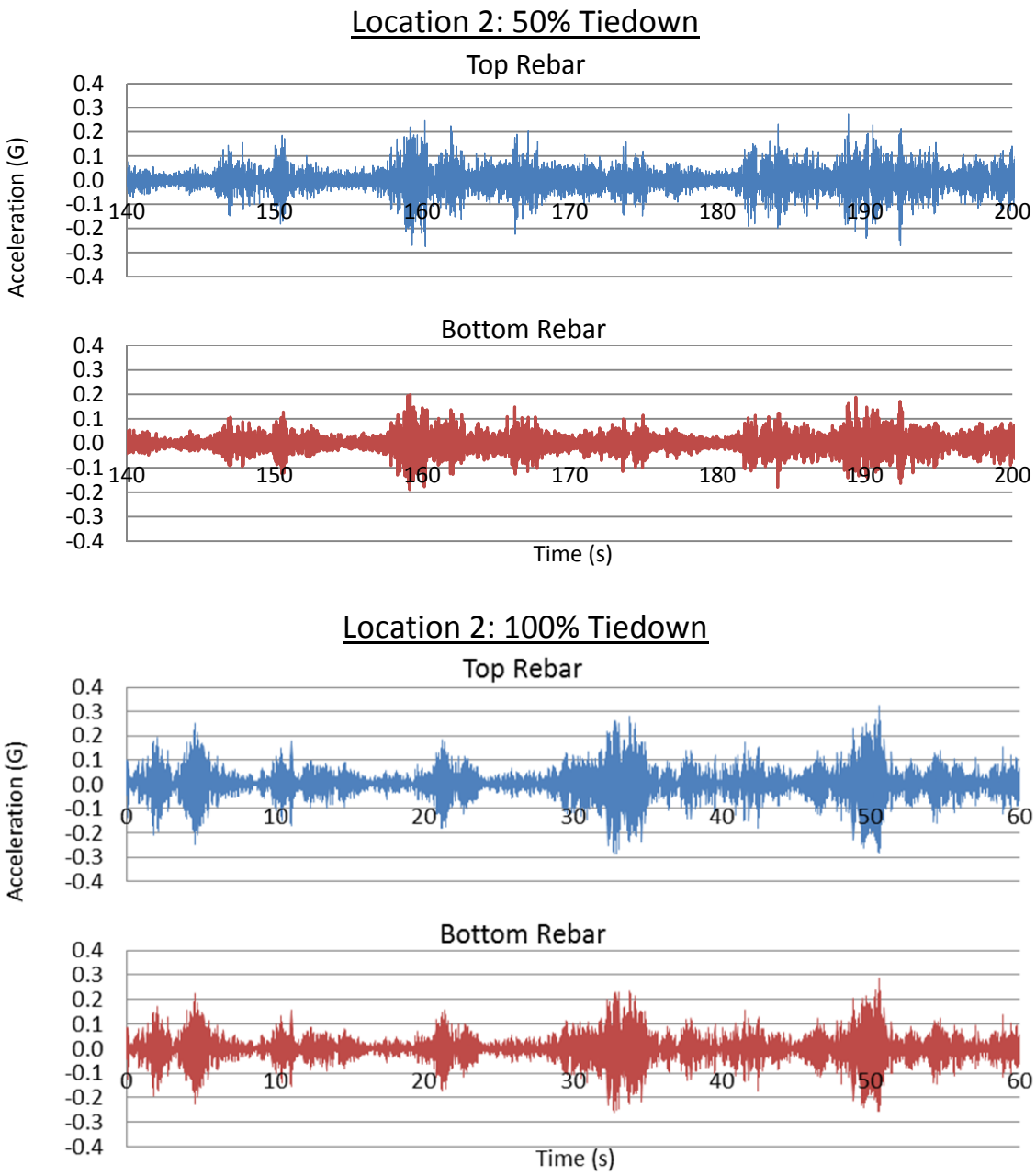

Figure 3.18 Location 2 tiedown comparison

3.4.3 Testing Procedure During the Deck Pour

The primary testing objective at the Hackensack River Bridge was to evaluate the bridge response during the critical concrete setting time, which is the first 3 hours after placement. As a result, the researchers developed a testing scheme to adequately monitor

Span N5 of the bridge in this time period along with periods immediately before and immediately after the pouring operations.

The general procedure was to conduct a separate test approximately every 5 to 10 feet of the deck span that was poured. Markers were placed at 10 foot intervals to allow the researchers to track the progress of the pour. A summary of the field tests is given in Table 3.4. The instrument sampling rates for all tests were 100 Hz. The first test was conducted 2 hours prior to the first concrete truck. The time between the first and last trucks was approximately 3.5 hours. The final test was conducted 3 hours after the last concrete truck. The LDV was only moved before and after the entire pour. During the actual pour, the LDV was used to monitor the R1 location on the WN5 girder (Figure 3.15). For the remaining tests, the LDV was arbitrarily located at either the R1 or R2 locations to compare the responses of the WN5 and West girders, respectively. The parameters in each test were the time, LDV location, and the length of the span that was already poured (measured from north to south). The time parameter is given in two forms: the absolute time of day, and the time relative to the instant that Sensor A2085 is covered by concrete at Location 2.

Table 3.4 Summary of Hackensack Bridge field test parameters

Test name	Description	Start time	Time relative to A2085 embedment (hh:mm)	Length of span poured [N-S] (feet)	Laser position (girder)
BP1	Before Pour	9:05 PM	-04:30	--	*West*
BP2	Before Pour	9:25 PM	-04:10	--	*West*
BP3	Before Pour	9:43 PM	-03:52	--	WN5
BP4	Before Pour	9:57 PM	-03:38	--	WN5
BP5	Before Pour	10:05 PM	-03:30	--	WN5
BP6	Before Pour	10:53 PM	-02:42	--	WN5
BP7	Before Pour	11:04 PM	-02:31	--	WN5
DP1	During Pour	11:22 PM	-02:13	0	WN5
DP2	During Pour	11:29 PM	-02:06	10	WN5
DP3	During Pour	11:48 PM	-01:47	20	WN5
DP4	During Pour	11:57 PM	-01:38	25	WN5
DP5	During Pour	12:08 AM	-01:27	30	WN5
DP6	During Pour	12:24 AM	-01:11	35	WN5
DP7	During Pour	12:27 AM	-01:08	40	WN5
DP8	During Pour	12:34 AM	-01:01	42	WN5
DP9	During Pour	12:46 AM	-00:49	52	WN5
DP10	During Pour	12:58 AM	-00:37	58	WN5
DP11	During Pour	1:09 AM	-00:34	62	WN5
DP12	During Pour	1:14 AM	-00:29	65	WN5
DP13	During Pour	1:20 AM	-00:23	75	WN5
DP14	During Pour	1:26 AM	-00:17	80	WN5
DP15	During Pour	1:35 AM	00:00	85	WN5
DP16	During Pour	1:49 AM	00:14	95	WN5
DP17	During Pour	1:57 AM	00:22	105	WN5
DP18	During Pour	2:09 AM	00:34	120	WN5
DP19	During Pour	2:17 AM	00:42	130	WN5
DP20	During Pour	2:30 AM	00:55	150	WN5
DP21	During Pour	2:39 AM	01:04	160	WN5
AP1	After Pour	3:00 AM	01:25	--	*West*
AP2	After Pour	3:35 AM	02:00	--	WN5
AP3	After Pour	4:02 AM	02:27	--	WN5
AP4	After Pour	4:32 AM	02:57	--	WN5
AP5	After Pour	5:10 AM	03:35	--	WN5
AP6	After Pour	5:34 AM	03:59	--	*West*

After the completion of the pour in test DP21, a basic assessment was made of the available data. Available with minimal processing were the acceleration results. Figure 3.19 gives the acceleration data for five consecutive tests, DP12 through DP16, which contain critical information on the behavior of the deck rebar during the pour. First, it can be seen that sensor A2086 at Location 1 is covered by concrete at some time near the end of DP12 and beginning of DP13, and the acceleration of that rebar is significantly reduced. Furthermore, it can be seen at the beginning of DP15 that there is a small spike it the acceleration at both locations, but it is significantly smaller at Location 1. Similarly, Sensor A2085 at Location 2 appears to have been covered by concrete near the beginning of DP15. The isolated spike accelerations over the course of DP15 were attributed to random construction activities on the deck since there were no corresponding spikes in the stringer acceleration. At the end of DP16, a small spike in the acceleration can be seen for both locations. This spike acceleration was slightly lower for Location 1 since the concrete had been poured earlier.

Other preliminary results include velocity, displacement, and strain. The responses for Girder WN5 at R1 and Sensor A2085 can be seen in Figure 3.20. The peak responses at 425 seconds are shown in more detail. Again, the problems of system synchronizations and sensor drift are evident. However, the period of forced vibration is shown to be short (< 4 seconds), and its boundaries are fairly easy to approximate by visual inspection. Lastly, it should be noted that the maximum rebar acceleration, girder acceleration, and girder displacements occurred at the same time in DP21. This is not always the case, and the selection of the time segments for analyses requires consideration of all the components of the response.

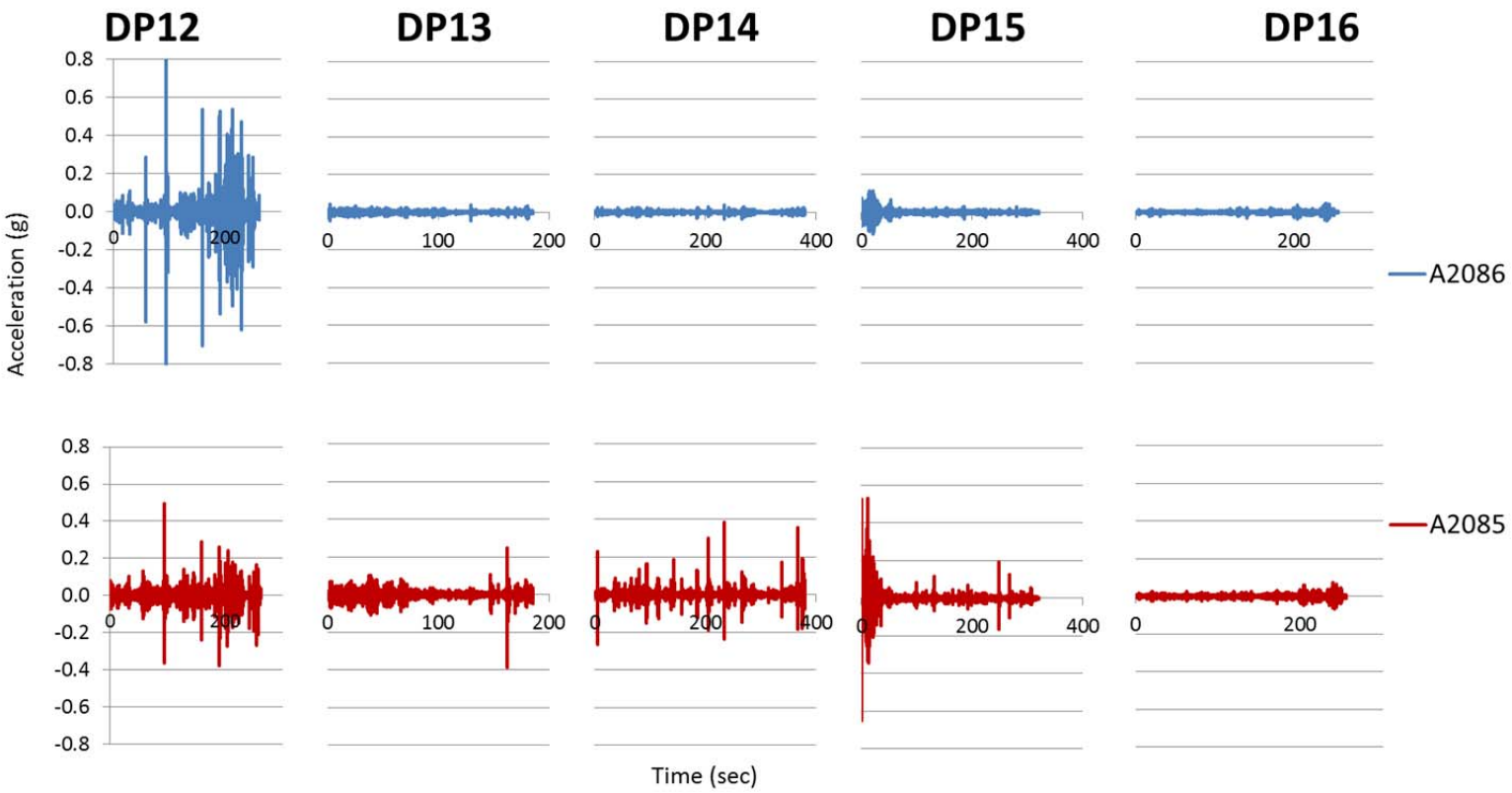

Figure 3.19 Dampening effect on rebar vibration

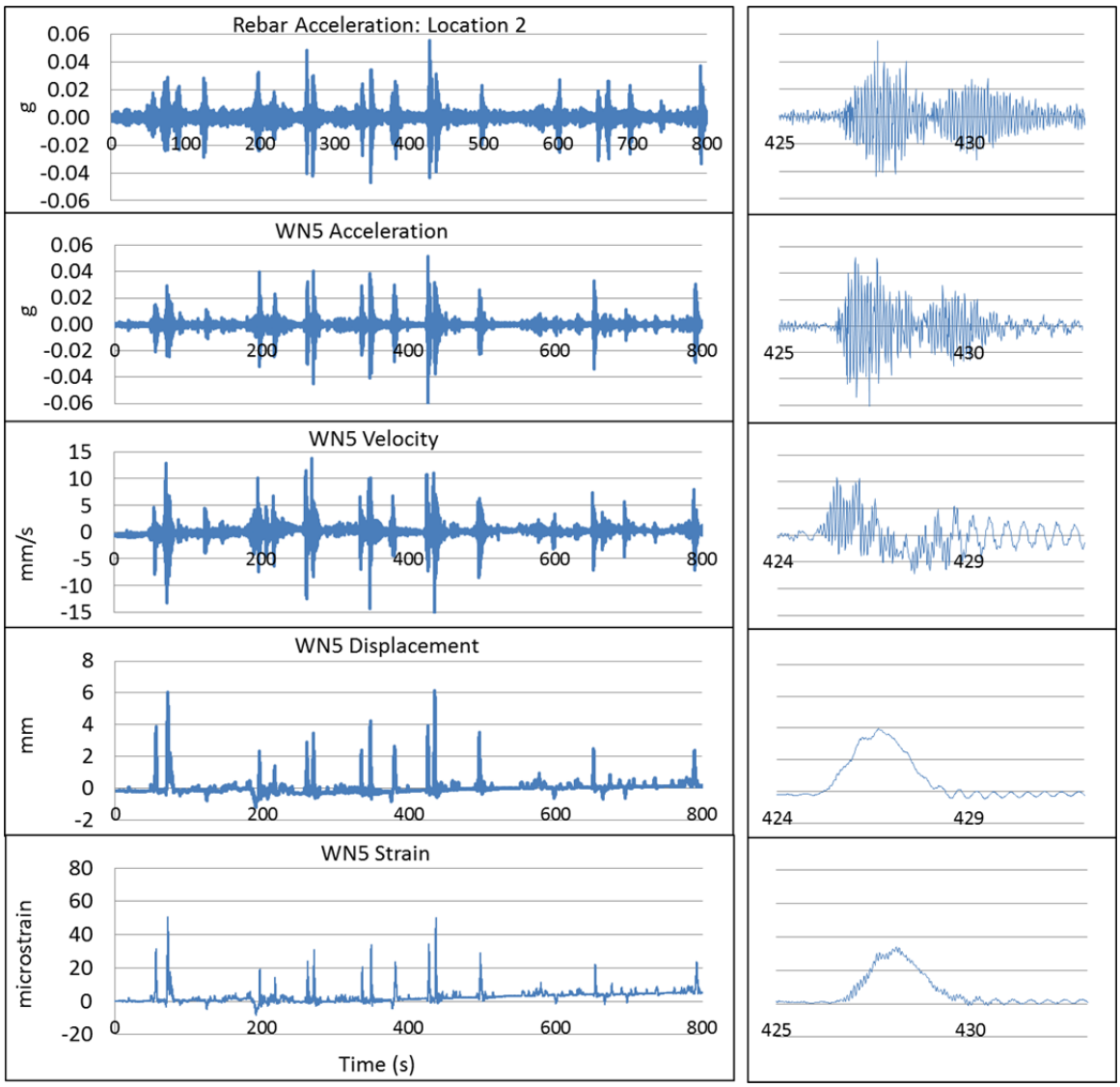

Figure 3.20 Bridge response for Test DP21

CHAPTER 4

SIGNAL PROCESSING AND ANALYSIS

4.1 INTRODUCTION

Analyses beyond the preliminary investigations in Chapter 3 require a significant amount of additional processing. Accurate estimates of the girder displacement from acceleration data, for example, require graphical analysis of peak accelerations and the boundaries of forced vibration. Numerical procedures must then be applied to evaluate the frequency spectra and perform double integration. A combination of theory, intuition, and experience are then required to interpret the results and associated errors.

The main subject in the study is the rebar velocity relative to the surrounding concrete, but many intermediate steps are involved to obtain this value. The process begins with the development of a numerical method to convert acceleration into displacement, and it is important to acknowledge all of the pitfalls discussed in Chapter 2. The girder response can be confirmed with experimental results from the LDV, so a comprehensive set of results are compiled for girder displacement estimates before proceeding to the next step.

Because an accurate displacement estimate implies an accurate velocity estimate, the conversion of acceleration to velocity in this study is actually preceded by the conversion of acceleration to displacement. Again, the availability of the LDV deems it

logical to begin with the girder response before evaluating the other structural components.

Success in predicting the girder velocities warrants confidence in most of the preceding assumptions and approximations. The boundaries of the forced vibration, for example, must be approximated intuitively by visual inspection. With no information on the stringer and rebar response other than acceleration, the assumed forced vibration boundaries must be carried over from the girder analysis. Along with direct measurements of displacement and velocity of the rebar, other methods of validating the results are available and explored.

4.2 CONVERSION FROM ACCELERATION TO DISPLACEMENT

The frequency domain method is used to convert acceleration to displacement. This choice was dependent on many factors. The time domain method, for example, requires several stages of correction and filtering. Furthermore, each stage requires some level of subjective input from the researcher. As was discussed in Chapter 2, each correction method includes several parameters that are not universally applicable. The result is also highly sensitive to the selection of parameters, such as filter cutoff frequencies. The start and end times of the baseline used for correction will also affect the result significantly.

The frequency domain method, on the other hand, requires fewer user inputs. Additionally, the frequency spectra offer a variety of insights, such as natural frequencies and noise identification (Shreve, 1995). One of the more significant advantages is that

the main component of the DC offset in the acceleration signal can be removed automatically by choosing to always suppress the first term in the FFT.

4.2.1 Numerical Algorithm in MATLAB

The conversion algorithm is based on Eq. 2.8. By dividing the FFT terms of acceleration by $-\omega^2 = -(2\pi f)^2$, the displacement can be determined in the frequency domain. Using the inverse FFT to convert back into the time domain, an estimate of the displacement signal is obtained.

$$D_k = -\frac{1}{(2\pi k)^2} A_k \qquad k = 0,1,2,...,(N-1) \tag{2.8}$$

The Matlab algorithm is as follows:

1) Input an even number of acceleration data points, the sampling rate, and the high-cut frequency.
2) Perform an FFT of the acceleration signal
3) Divide the FFT of acceleration by the negative square of frequency in radians ($-\omega^2$)
4) Suppress the first term in the FFT to remove the DC component
5) Apply a low-pass filter to remove the dynamic components of displacement
6) Perform an inverse FFT on the signal; the real part of the inverse FFT is the time-waveform of displacement
7) Remove a constant offset, taken as the first term in the displacement vector, to account for non-zero initial displacement
8) Differentiate the displacement to obtain velocity

```
%Step(1)
%INPUTS
%       a = acceleration(g)
%       fs = sampling rate(Hz)
%       cut = cutoff frequency(Hz)

a = a*9.81*1000;                                % mm/s^2
k = length(a);
f = fs*[(0:1:k/2-1) (k/2:-1:1)]/k;              % Hz
w = 2*pi*f;                                     % rad
w2 = w .* w;

%Step(2)
A = fft(a);

%Step(3)
D = A ./ (-w2);

%Step(4)
D(1) = 0;

%Step(5)
Dstatic = D;
Dstatic(f>cut) = 0;

%Step(6)
dstatic = ifft(Dstatic);
dstatic = real(dstatic);
d = ifft(D);
d = real(d);

%Step(7)
dstatic = dstatic – dstatic(1);                 % mm
d = d - d(1);                                   % mm

%Step(8)
tstep = 1/fs;
for count=1:k-1
   v(k)=(d(count+1)-d(count))/tstep;            % mm/s
end

%OUTPUTS
%       Acceleration (mm/s^2): a
%       Velocity (mm/s): v
%       Displacement (mm): d
%       Pseudo-static displacement (mm): dstatic
```

4.2.2 Application on the 7A Bridge

The algorithm was applied to data from the 7A Bridge, where the controlled testing conditions allowed for greater fine-tuning of the procedure. After routine data processing of the raw data to obtain graphs of acceleration, velocity, displacement, and strain, a comparison must be made of the displacements and strains in order to validate the results. This is critical because the selection of the integration interval is dependent on the perceived boundaries of forced and free vibrations. Since the 7A bridge is has two continuous spans, the segment of forced vibration is essentially twice as long. Integrating this whole segment at once will result in large errors. Therefore, the integration is performed on each span separately. This requires the selection of three different times, t_1, t_2, and t_3 that define the boundaries of forced vibration. The first parameter, t_1, is selected where initial conditions are equal to zero. With regards to error, it is more conservative to shift t_1 to the left (i.e., include more of the initial free vibration period), because a shift too far to the right will result in non-zero initial conditions.

Figure 4.1 shows typical results for displacement estimates. Interval A is defined as the optimal configuration of t_1, t_2, and t_3, based on the approach of isolating the forced vibration. The effect of small errors in determining the bounds t_1 and t_2 are evaluated by truncating the integration interval by 5% at each end. In other words, the integration is being performed on the inner 90% portion of the forced vibration segment corresponding to Span 1. This interval is referred to as Interval S, since the interval is "shorter," and it is defined by:

$$t_{1error} = t_1 + 0.05 * (t_2 - t_1)$$
$$t_{2error} = t_2 - 0.05 * (t_2 - t_1)$$
$$t_{3error} = t_3$$

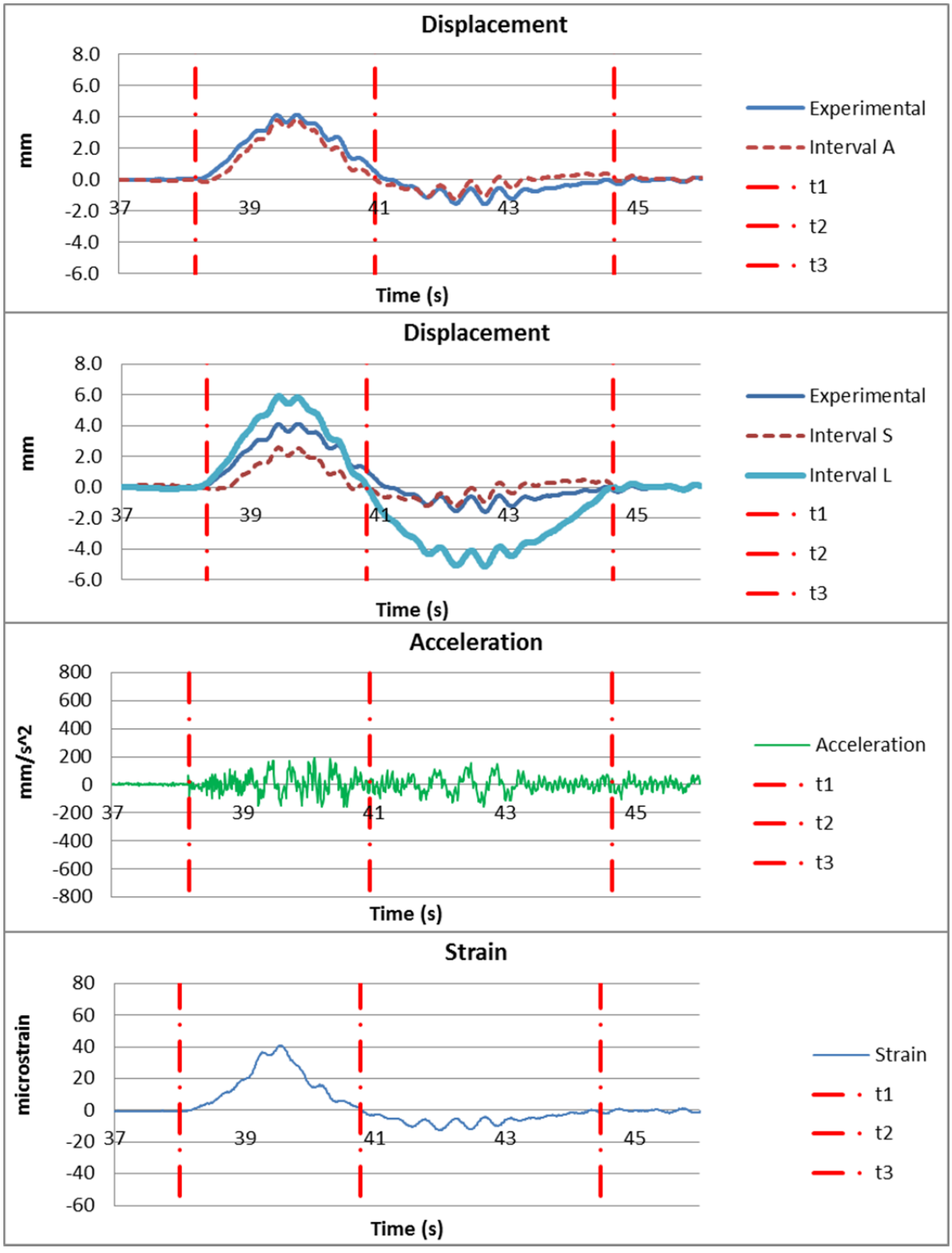

Figure 4.1 Displacement estimates for Test G35

A third interval involves the integration of the entire forced vibration segment, corresponding to the loading of both Span 1 and Span 2. This "longer" interval is referred to as Interval L.

The large error in the Interval L displacement estimate demonstrates the parabolic amplifying effect of the $-\omega^2$ in the denominator as the integration interval gets larger. For Interval S, the truncation of the forced vibration period seems to have a diminishing effect on the peak displacement estimate. In the frequency domain, the effect of the truncation is a removal of significant contributing frequency components. In the time domain, there is simply less area under the curve. A comparison of the spectral frequencies of the LDV and the estimated displacement show that Interval A accurately captures the main frequency components of the displacement response.

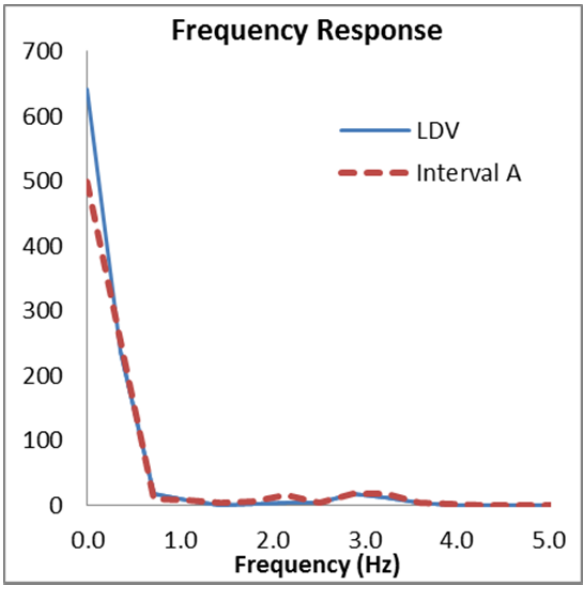

Figure 4.2 Spectral frequency of displacement for Test G35

4.2.3 Application on the Hackensack River Bridge

The signal processing of the 7A Bridge data provided an understanding of the algorithm and the sources of error. The conditions on the Hackensack River Bridge pose unique advantages and disadvantages over those at the 7A Bridge. Although the bridge is simple supported and the integration intervals are shorter, it is open to normal vehicular traffic. This increases the difficulty of isolating a large live load event on the response records. As a result, the estimation of displacements on the bridge required more trial and error.

Because the girder displacement was only the first part of the investigation on the bridge, the general analytical procedure was more complicated. The first step, again, is to compare the strains with the LDV displacements to validate the results. Next, peaks in the girder displacement signal are compared to peaks in the stringer and rebar acceleration signals in order to select a loading event to evaluate. Several conditions must be met before numerical analysis is performed. The loading event, as observed in the displacement graphs, must be isolated enough such that the forced vibration boundaries can be easily identified. Also, the event must cause a large acceleration the rebar (Sensor A2085) comparable to other large peaks in the record. Lastly, the stringer response must be observed to be similar to the rebar response. The rebar is more sensitive to accelerations than the girders and stringers, so the possibility of random noise on the deck must be considered.

As shown in Figure 3.20, the time segment between 424s and 433s in DP21 meets all the criteria for analysis. The estimated displacements are shown in Figure 4.3. The behavior of errors is similar to the 7A Bridge. In this case, the Interval L contains not

only the forced vibration segment, but the free vibration segments before and after the loading as well. The total lengths of the intervals vary from test to test, ranging from 6-8 seconds. The approach is to select an interval just large enough to clearly show the periods of free vibration on either side of the forced vibration segment. This allows for more trial and error in selecting the optimum integration interval.

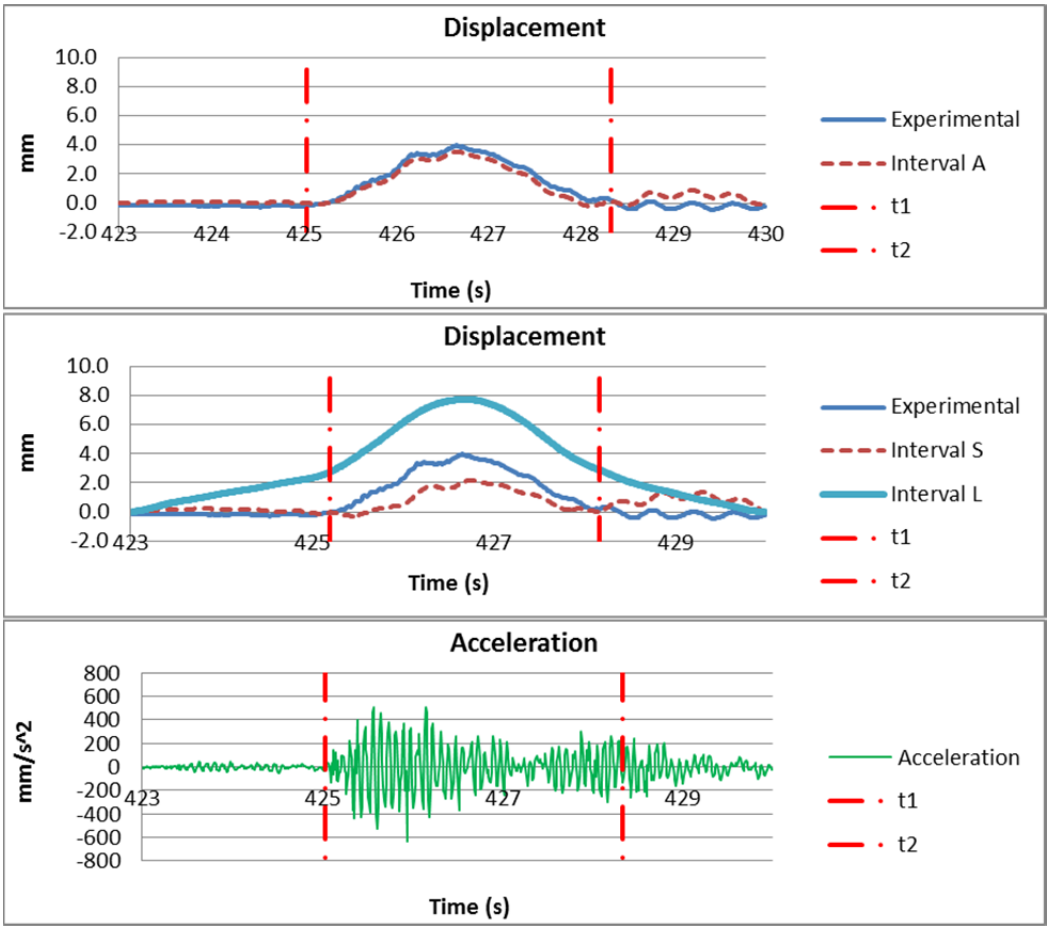

Figure 4.3 Displacement estimates for Test DP21

The error using Interval L is once again substantial. A significant amount of low-frequency noise is being added to the signal, and the amplification is parabolic. The truncated period in Interval S would seem like a reasonable choice of boundaries based on visual inspection, but there is significant error resulting from only a 10% truncation.

This demonstrates once again that it is more conservative to extend the interval into the free vibration portions rather than truncate the signal. The introduction of a non-zero initial condition is also of concern because the algorithm is based on the assumption of a zero initial condition.

The result for Interval A is reasonable, and the velocity is obtained next by differentiation (Figure 4.4). A very slight rotation can be seen in the estimated velocity. Since the displacement is amplified in a quadratic manner by noise, differentiation produces linear error in the velocity. Nevertheless, the velocity estimate is show to be more accurate than the displacement estimate.

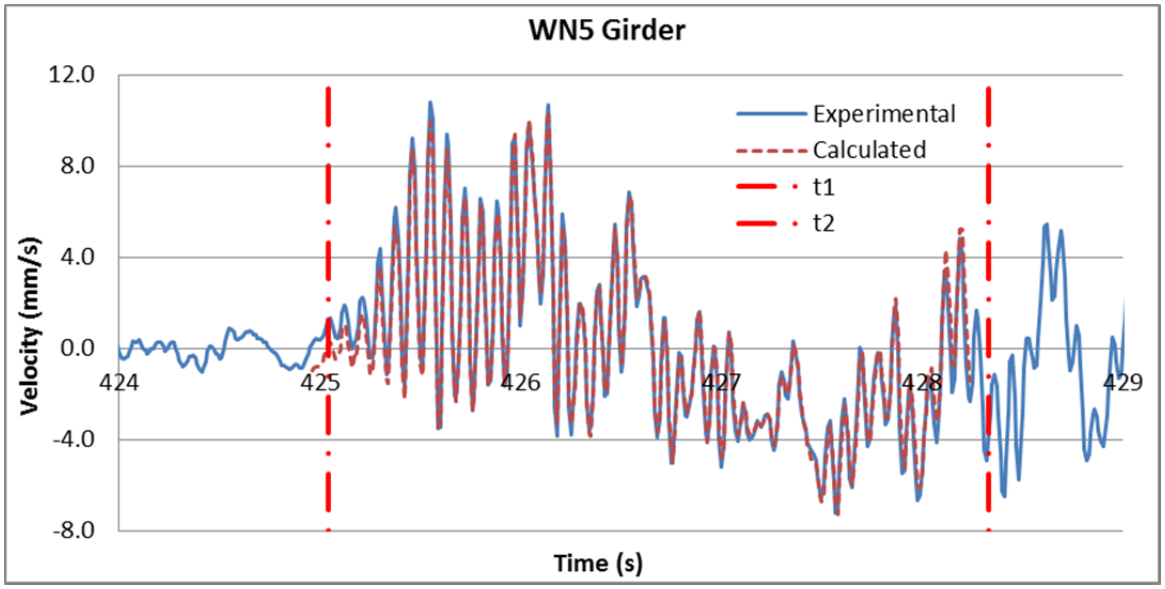

Figure 4.4 Girder velocity estimate for Test DP21

Finally, the rebar and stringer responses are evaluated (Figure 4.5). This segment in the record corresponds to 71 minutes after the embedment of the rebar sensor in the concrete deck. From these results, it seems that the concrete has had sufficient time to set around the rebar, such that the rebar vibration is nearly harmonic with the stringer. By

extension, the rebar vibration should be harmonic with the surrounding concrete deck as well. The displacement estimates seem to suggest a difference in the rebar and stringer motions, but this can be attributed to errors in the estimate. Still, the displacement error is reasonably small. More importantly, the previous example showed that the velocity is estimated more accurately than the displacement. Because of the quality of the results, a more comprehensive analysis of the available data was performed. These are discussed in detail in Chapter 5.

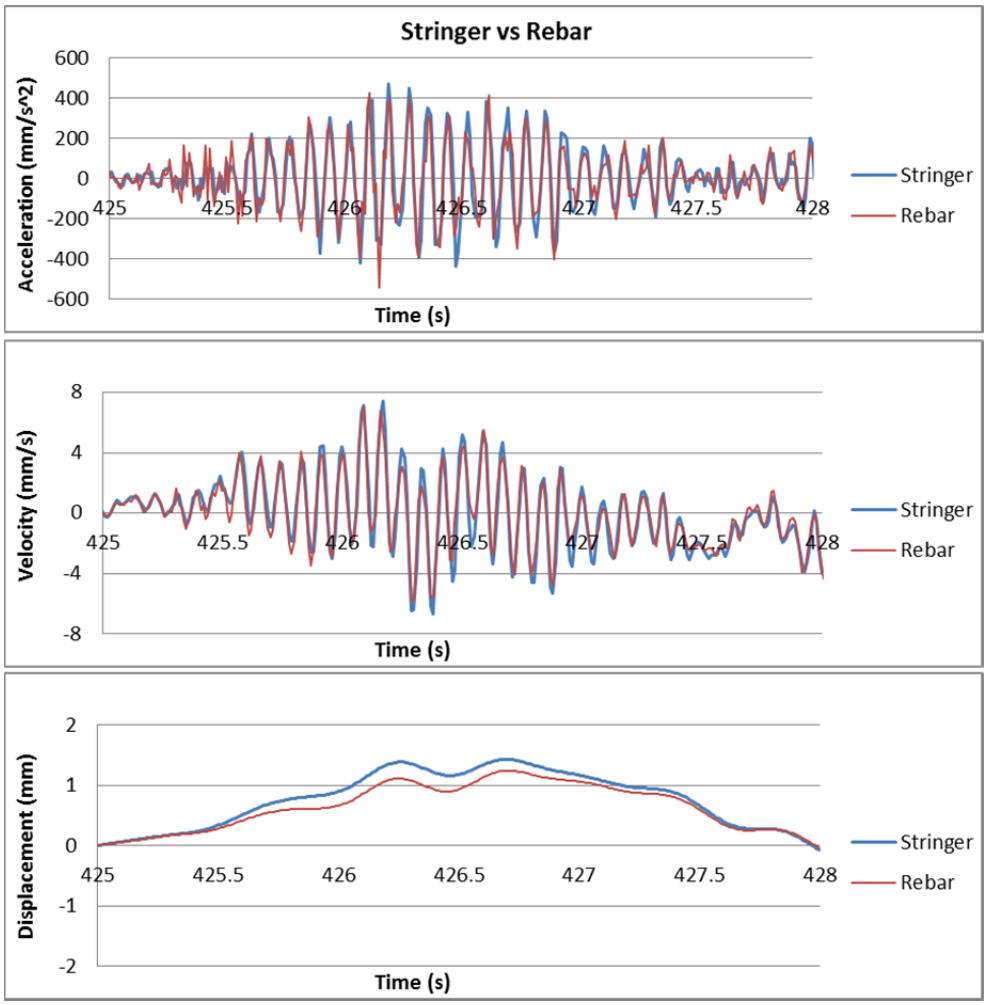

Figure 4.5 Stringer and rebar response for Test DP21

CHAPTER 5

RESULTS AND DISCUSSION

5.1 ANALYSIS OF THE 7A BRIDGE

The tests for analysis were selected for truck speeds of at least 20 mph, since the integration periods for 5 mph would be over 20 seconds long. The displacement time histories were estimated from the mean-removed accelerometer data, and the length of the histories were selected such that the initial free vibration, the forced vibration, and the final free vibration segments were clearly defined. The analysis of the results focuses primarily on the accuracy of the peak displacement estimates.

5.1.1 Truck on Span 1 (North Abutment to Pier)

A summary of the displacement estimates is given in Table 5.1. The largest displacements measured on Girders 1, 3, and 5, were 4.62mm, 4.37mm, and 3.35mm, respectively. The truck times on Span 1 ranged from 2.71 to 6.65 seconds. The root-mean-squared error is defined as:

$$RMSE = \sqrt{\frac{1}{n}\sum_{i=1}^{n}(\hat{Y}_i - Y_i)^2} \tag{5.1}$$

where $\hat{Y}_i$ are displacement estimates and Y_i are the true values, taken to be the same as the LDV measurements.

As previously noted, when Interval S is used to define the forced vibration segment in the algorithm, the predicted displacement typically underestimates the true displacement and the mean percentage error was negative. When using Interval L, however, the mean percentage error was positive, corresponding to an overestimate. Interval A, assumed to closely approximate the forced vibration segment, was shown to give accurate results with an average absolute error of 5.8%. Because the start time, t_1, was selected conservatively to include some of the initial free vibration segment, Interval A typically resulted in positive rather than negative error.

Table 5.1 Peak displacement estimates with truck on Span 1

Test	Speed, mph	Load duration, s	LDV Peak Displacement, mm	Error, %		
				Interval A	Interval S	Interval L
G14	20	5.45	4.62	-5.8	73.5	196.7
G15	40	2.87	4.44	-0.3	-55.9	-49.3
G16	40	2.89	4.51	10.1	-37.2	-8.1
G33	25	4.57	4.37	16.4	11.9	81.3
G34	20	5.41	4.19	8.5	47.2	41.0
G35	40	2.77	4.11	-7.7	-37.2	44.3
G36	40	2.71	4.09	-5.6	-43.9	42.3
G37	20	5.41	4.10	7.4	48.2	-2.2
G3_15	40	2.87	4.11	0.8	-17.1	18.2
G3_16	40	2.89	4.11	11.4	-36.9	111.0
G3_53	40	3.01	4.11	0.5	-6.7	85.8
G52	20	6.65	3.35	0.5	-31.3	52.6
G53	40	3.01	3.25	0.4	-34.7	-20.4
Max overestimate, %				16.4	73.5	196.7
Max underestimate, %				-7.7	-55.9	-49.3
Mean percentage error				2.8	-9.2	45.6
Mean absolute percentage error				5.8	36.6	68.0
Root-mean-square error				0.075	0.942	2.519

To check if the error is correlated to either the length of the integration interval or the magnitude of the peak displacement, the error percentages are plotted against each of these parameters in Figure 5.1. It can be seen that for any particular value of load

duration or peak displacement, the errors are not inconsistent. For example, load durations of approximately 3 seconds result in errors varying from -6.7% to -55.9% using Interval S. For peak displacements ear 4 mm, the errors using Interval L vary from -2.2% to 110%. This affirms the notion that the errors result from a complex combination of factors such as noise, integration bounds, and transducer drift.

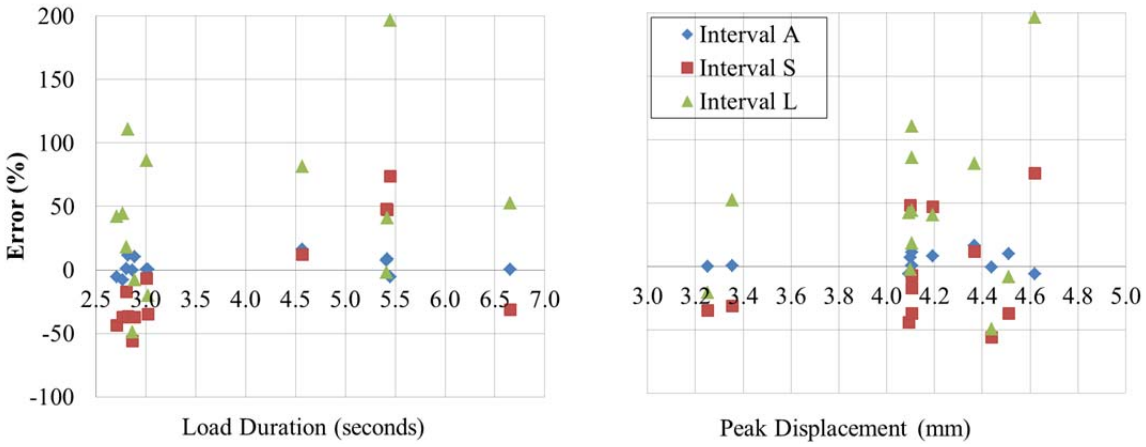

Figure 5.1 Errors in displacement estimate (Span 1 loaded)

A typical good result is shown in Figure 5.2. The correct shape and magnitude of displacement were accurately reproduced for the 14 second segment of the history. Interval S gave a low estimate, and Interval L gave a high estimate, which is consistent with the overall trend of errors across all tests. Most importantly, this test had the longest load duration for Span 1, so that the conversion of displacement from acceleration was applied on a very long time interval. This truck was traveling below 20 mph on a 150 ft. span, whereas the ideal situation would involve significantly higher speeds and/or shorter spans. This suggests that the algorithm can be effective for a wide array of live load speeds and bridge span lengths.

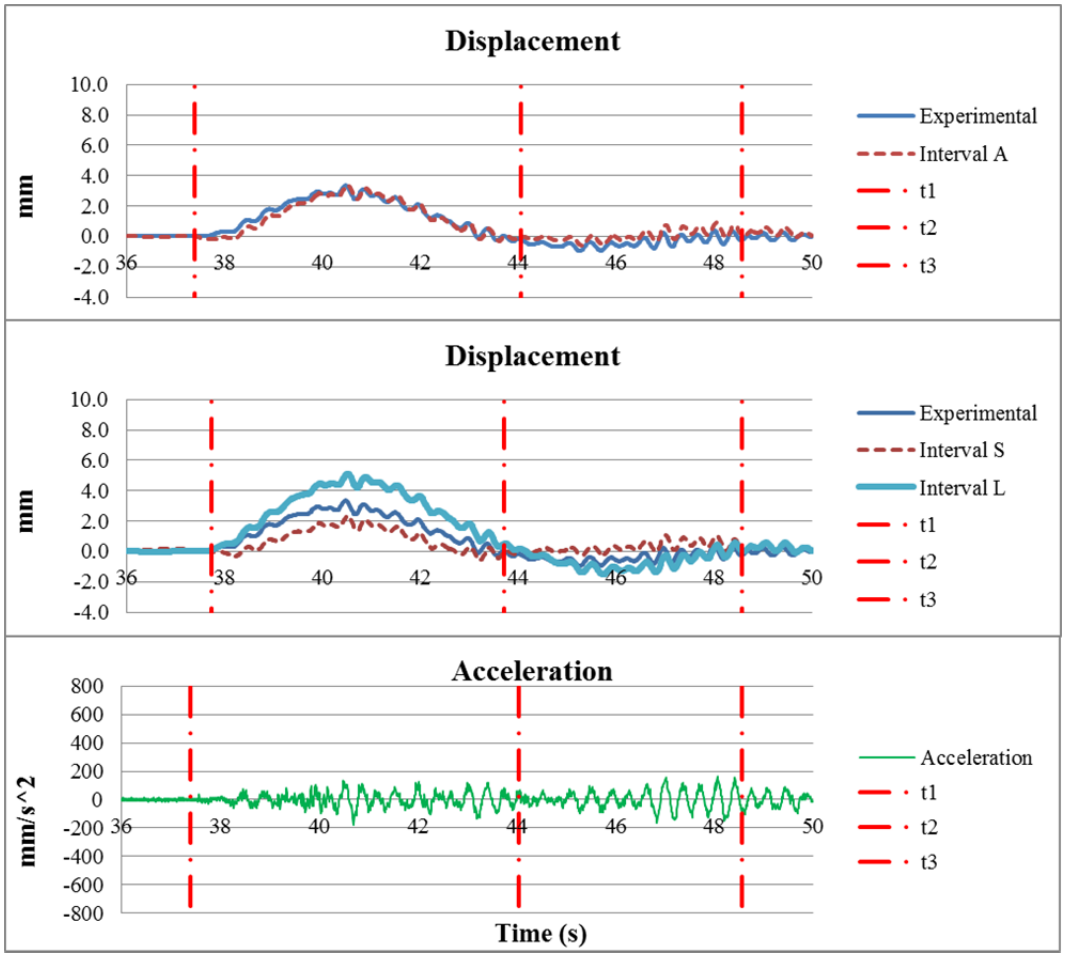

Figure 5.2 Displacement estimates for Test G52

A typical poor result is shown in Figure 5.3. Although Interval A gave very accurate estimates, Intervals S and L resulted in severely distorted displacement signals. Additionally, Interval L did not provide an overestimate, which is inconsistent with the other tests in general. The most concerning issue, however, is that the Interval S truncation of only 5 percent of the record at each end of the forced vibration segment resulted in a very different displacement signal than the one predicted with Interval A. Again, this demonstrates the complex interplay between the error-contributing factors. One such factor is the unknown initial displacement, especially at t_2, when the truck is directly over the pier. There is no free vibration segment here to provide leeway in

selecting a t_2 at zero initial displacement, and a non-zero initial value resulted in significant error in the displacement when Span 2 was loaded.

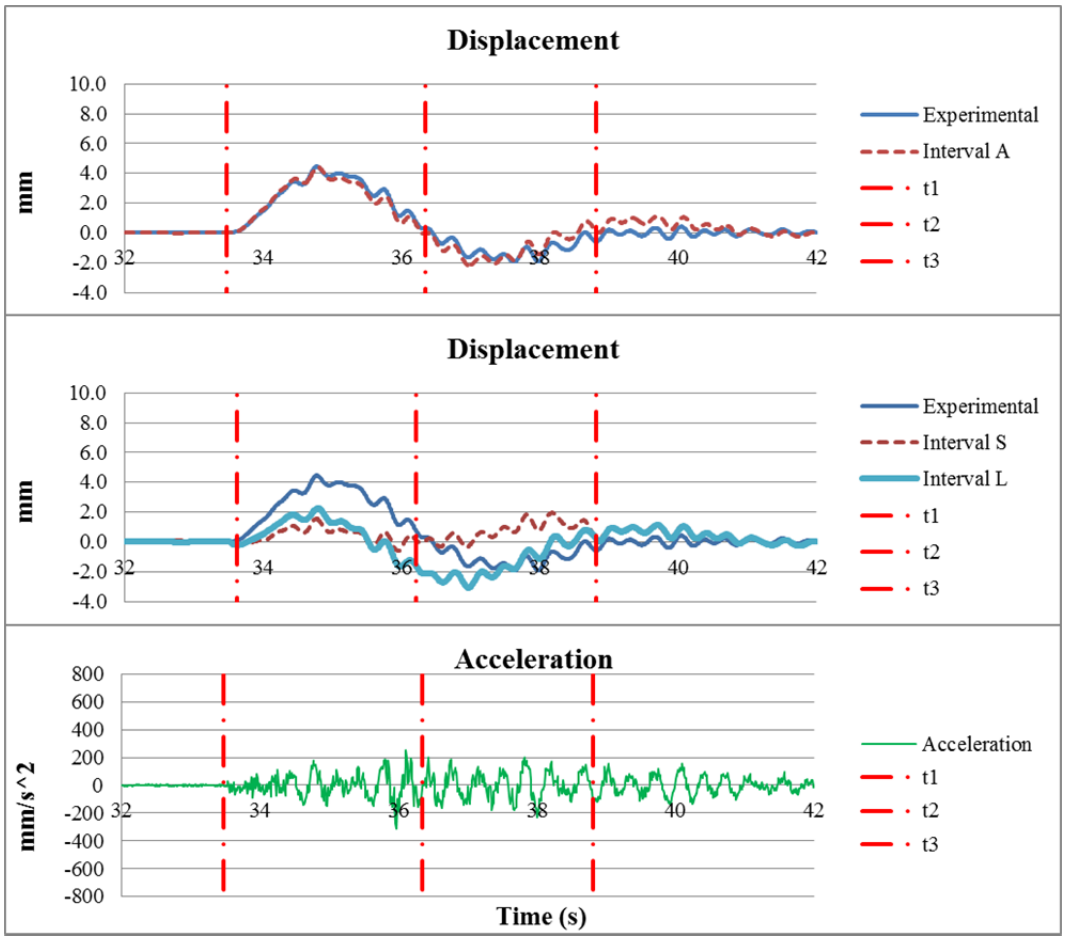

Figure 5.3 Displacement estimates for Test G15

5.1.2 Truck on Span 2 (Pier to South Abutment)

When the truck reaches Span 2, there is a negative moment effect on Span 1, causing a tendency to produce upward deflections in cambering manner. In this discussion, positive error corresponds to an overestimation of this camber, while negative error corresponds to an underestimation. However, the magnitudes of displacement will still be treated as positive when downward.

A summary of the deflections is given in Table 5.2 for the period when the truck is on Span 2. The maximum load duration was 5.26 seconds. The largest measured deflection was -2.04 on Girder 1, and the smallest was -0.95 on Girder 5. This is consistent with the findings for Span 1 loading.

Table 5.2 Peak displacement estimates with truck on Span 2

Test	Speed, mph	Load duration, s	LDV Peak Displacement, mm	Error, %		
				Interval A	Interval S	Interval L
G14	20	5.26	-2.04	42.0	252.9	892.9
G15	40	2.46	-1.95	12.8	-69.3	58.5
G16	40	3.36	-1.82	27.5	-49.6	88.4
G33	25	5.22	-1.55	59.7	154.9	703.1
G34	20	5.04	-1.57	27.2	144.8	51.2
G35	40	3.70	-1.58	-20.5	-23.2	224.3
G36	40	3.46	-1.42	-4.1	-55.3	224.8
G37	20	4.52	-1.62	-6.9	224.2	618.7
G3_15	40	2.36	-1.58	37.9	51.5	163.0
G3_16	40	2.74	-1.58	-45.3	-73.1	35.0
G3_53	40	2.52	-1.58	-82.3	-38.9	55.0
G52	20	4.52	-0.95	-38.2	-38.4	59.2
G53	40	2.52	-1.01	47.6	-10.7	97.0
Max overestimate, %				59.7	252.9	892.9
Max underestimate, %				-82.3	-73.1	35.0
Mean percentage error				4.4	36.2	251.6
Mean absolute percentage error				34.8	91.3	251.6
Root-mean-square error				0.628	2.091	6.736

The mean percentage errors for Interval S are misleading in the sense that they suggest a trend of overestimation. A plot of the error percentages in Figure 5.4 shows that Interval S typically underestimated the deflection. This is consistent with the Span 1 loading effects, and it is again related to the summation of the area under the curve. In the first forced vibration segment, the truncation by Interval S causes a reduction in the area under the curve because positive area is being removed. In the second forced vibration segment, Interval S appends rather than truncates the segment. However, the area under the curve of this appended segment is of opposite sign, and causes a reducing

effect in the camber estimate when integrating. In the frequency domain conversion, the contributing components of the Span 1 loading are being included in the FFT and inverse FFT, and the camber is underestimated.

Interval A was far less accurate for the second forced vibration segment than the first, but the errors are reasonable with a mean absolute error of 34.8%. Interval A typically underestimated the measured displacement, while Interval L always produced an underestimate. However, the errors for Interval L were much more severe. Figure 5.5 shows the two worst cases for the camber estimate using Interval L. The two tests in the figure, Tests G14 and G33, also have the longest load durations for Span 2. Still, other tests such as G34 and G52 have similar load durations without nearly the same magnitudes of error. A possible explanation is the resonance of low-frequency noise signals. In this hypothetical scenario, as the truck leaves Span 1, it passes over a node in the signal before entering Span 2, when additional noise may be created in Span 1. In the frequency spectrum, these noise components accumulate over the long test duration and are amplified by the ω^2 factor in the conversion from acceleration to displacement. Since resonance is a random occurrence, this would explain why large errors occur in some tests and not in others of the same duration.

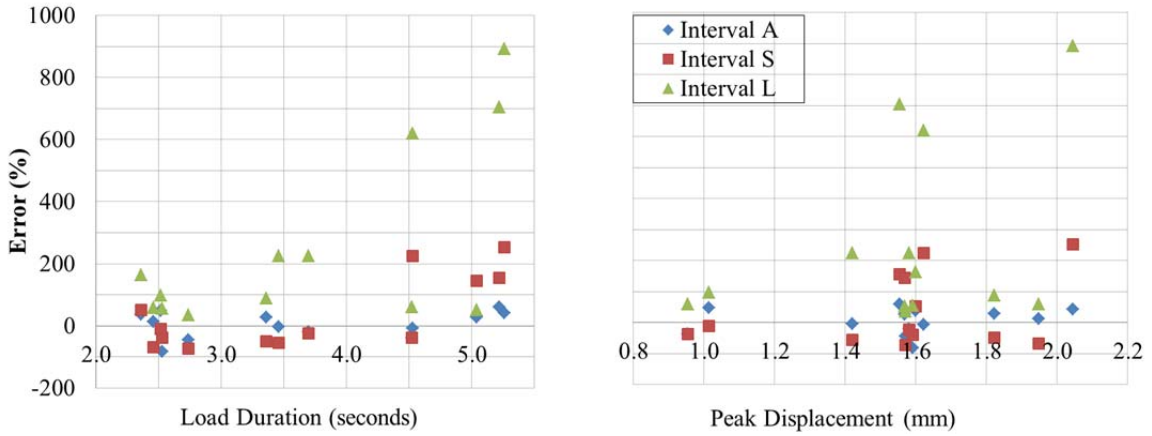

Figure 5.4 Errors in displacement estimate (Span 2 loaded)

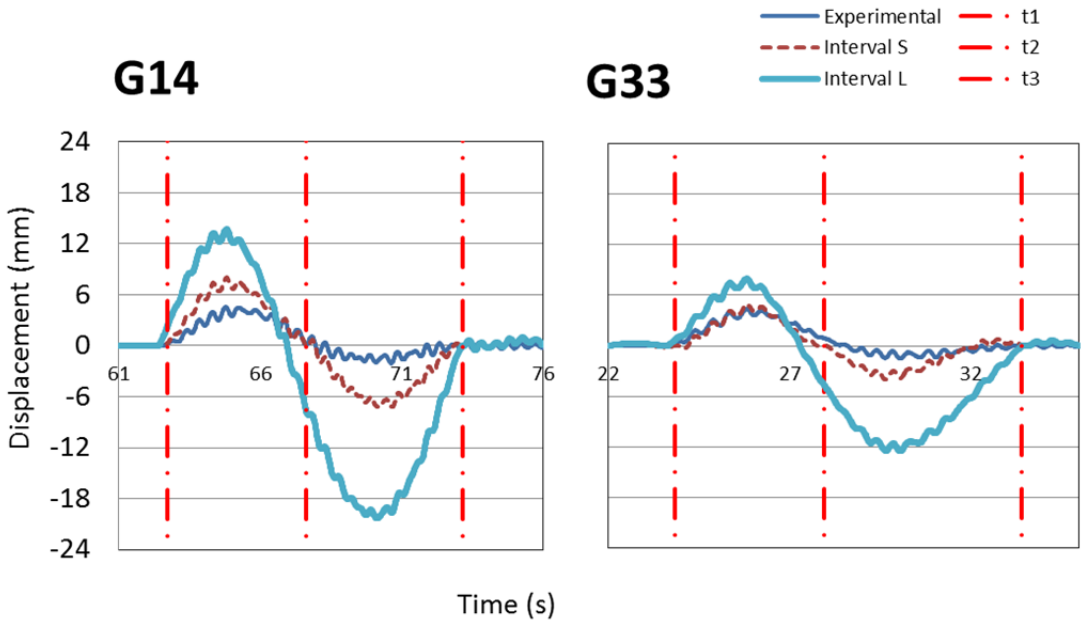

Figure 5.5 Displacement estimates for Tests G14 and G33

5.2 ANALYSIS OF THE HACKENSACK BRIDGE

The results of interest from the Hackensack Bridge analysis are girder displacement, girder velocity, stringer velocity, and rebar velocity. The primary challenge was to find periods of isolated forced response in the midst of real highway traffic on the bridge. Additionally, the bounds of forced vibration were difficult to deduce by observation. To overcome these challenges, a significant amount of subjective analysis and trial and error methods were utilized.

5.2.1 Estimation of Girder Displacements

Analysis of the Hackensack Bridge girder response was approached in a similar manner as that of the 7A Bridge. Interval A represents the optimal selection of t_1 and t_2 as boundaries of the forced vibration region, while Interval S represents 5% truncation at the beginning and end of Interval A. Interval L here is different, such that the conversion to displacement is performed on the free and forced vibration segments at the same time.

The results of 17 tests are shown in Table 5.3. The minimum and maximum load durations were 2.55 and 5.29 seconds. For the 167 ft. span, these correspond to vehicular speeds ranging from 20 to 45 mph. The peak displacements measured by the LDV range from 2.93 to 7.43 mm.

The absolute percentage errors for Interval A were consistent, but they were typically higher than those at the 7A Bridge. The average absolute error was 10.4%, while it was 5.8% for the 7A Bridge. This can be attributed to the random noise on the bridge that made it difficult to discern the forced vibration boundaries. Interval S consistently produced underestimates, and Interval L consistently resulted in

overestimates. This is consistent with the observed patterns in previous sections. Plotting the errors against the load duration and peak displacements (Figure 5.6), a fairly good scatter is observed, so there is no correlation suspected.

Table 5.3 Summary of peak displacement estimates

Test	Time relative to embedment, minutes	Load duration, sec	LDV Peak Displacement, mm	Error, %		
				Interval A	Interval S	Interval L
BP3	-230	4.41	6.01	-10.6	-25.9	37.8
BP5	-209	5.29	3.12	13.1	23.5	86.3
DP3	-105	4.11	5.38	14.1	-42.8	-72.8
DP7	-67	3.09	6.45	-10.0	-14.1	-5.4
DP17	22	3.30	6.34	12.1	-8.3	61.9
DP17	25	3.99	4.90	0.1	-12.0	-11.8
DP17	26	3.27	4.44	8.0	-64.8	14.6
DP19	48	3.35	4.21	-13.3	-38.0	-10.7
DP19	49	3.57	3.62	11.2	-10.3	82.0
DP21	68	2.55	2.93	1.6	31.6	0.3
DP21	71	3.29	3.96	-10.9	-44.6	95.3
AP2	121	3.01	6.55	-10.9	-19.0	34.6
AP2	125	3.15	5.80	11.3	-19.2	22.4
AP3	149	3.52	4.81	18.6	86.9	130.2
AP4	181	3.51	6.56	9.9	-44.1	-33.0
AP5	223	4.13	7.43	10.2	9.8	8.6
AP6	247	3.67	5.46	11.3	44.9	58.8
Max overestimate, %				18.6	86.9	130.2
Max underestimate, %				-13.3	-64.8	-72.8
Mean percentage error				3.9	-8.6	29.4
Mean absolute percentage error				10.4	31.7	45.1
Root-mean-square error				0.597	1.834	2.670

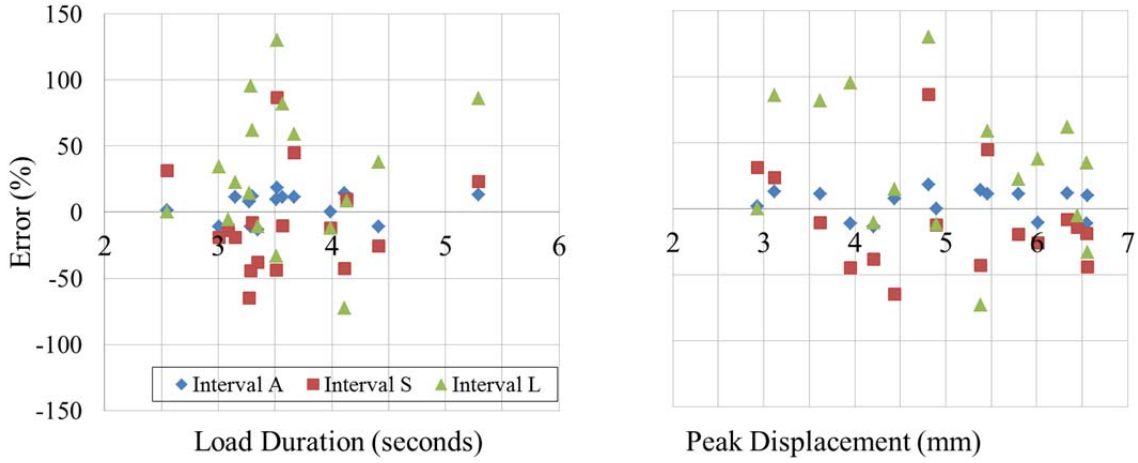

Figure 5.6 Errors in displacement estimate

A typical good result is shown in Figure 5.7. Interval A accurately reproduced the actual displacement history, including free and forced vibration segments. Interval S gave a low estimate with -19% error, and Interval L gave a high estimate with 22% error. A typical poor result for Test DP3 is shown in Figure 5.8. Although the estimated displacement signal was accurate with Interval A, there were wild, unexpected distortions in the estimates for Intervals S and L. In this example, it is very difficult to discern the free and forced vibration boundaries by simply inspecting a plot of the measured displacement or strain history. It is very likely that this forced vibration event was not due to a single heavy vehicle. With two lanes open and typical late evening traffic, there could have been a combination of vehicles that produced this response. Truncating the beginning or end of the assumed forced vibration segment of Interval A may remove contributing components of the response, while appending too much of the free vibration segments will cause the signal to be dominated by noise and free vibration energy. Cases like Figure 5.8 may be typical in normal traffic, creating a significant challenge in accurately predicting displacements.

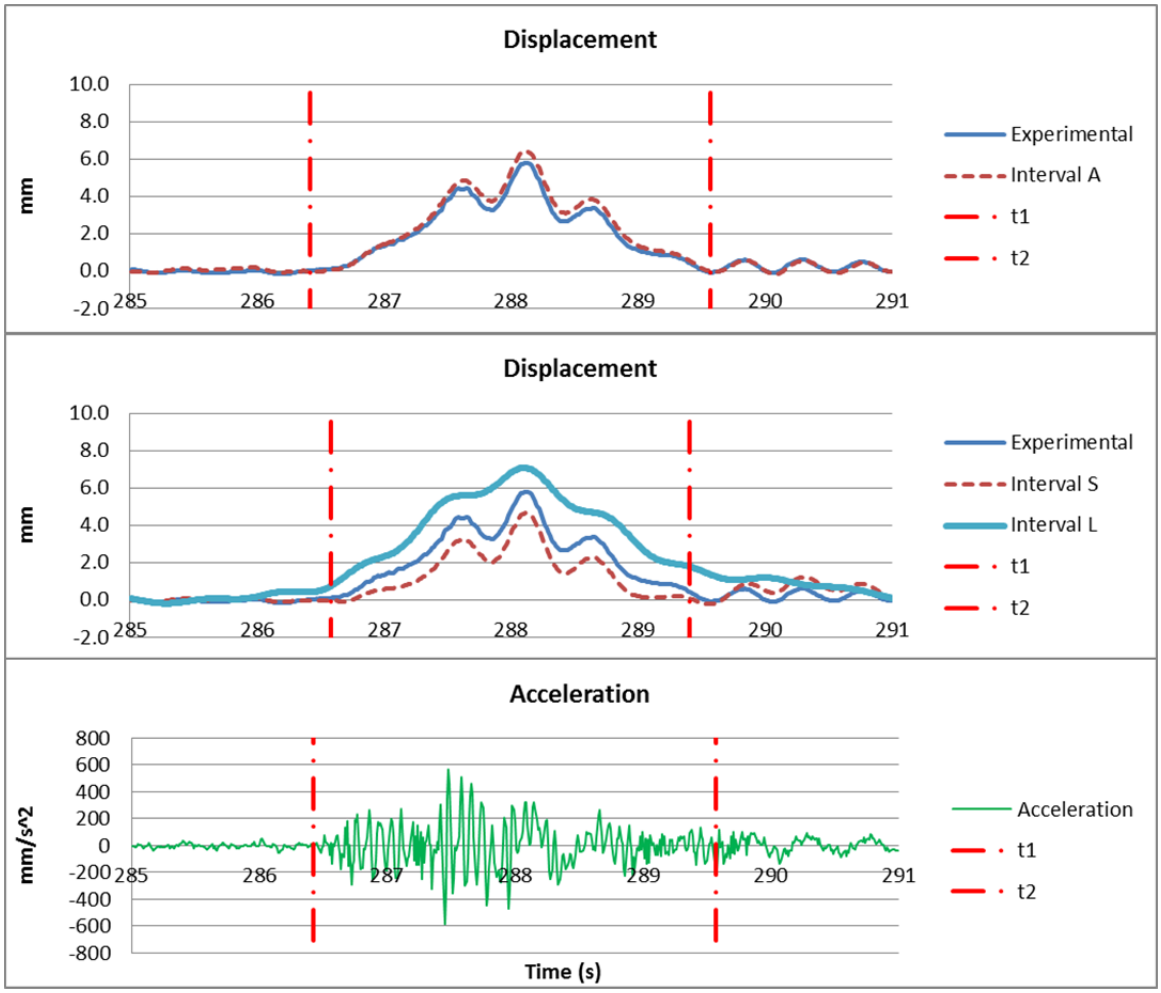

Figure 5.7 Displacement estimates for Test AP2

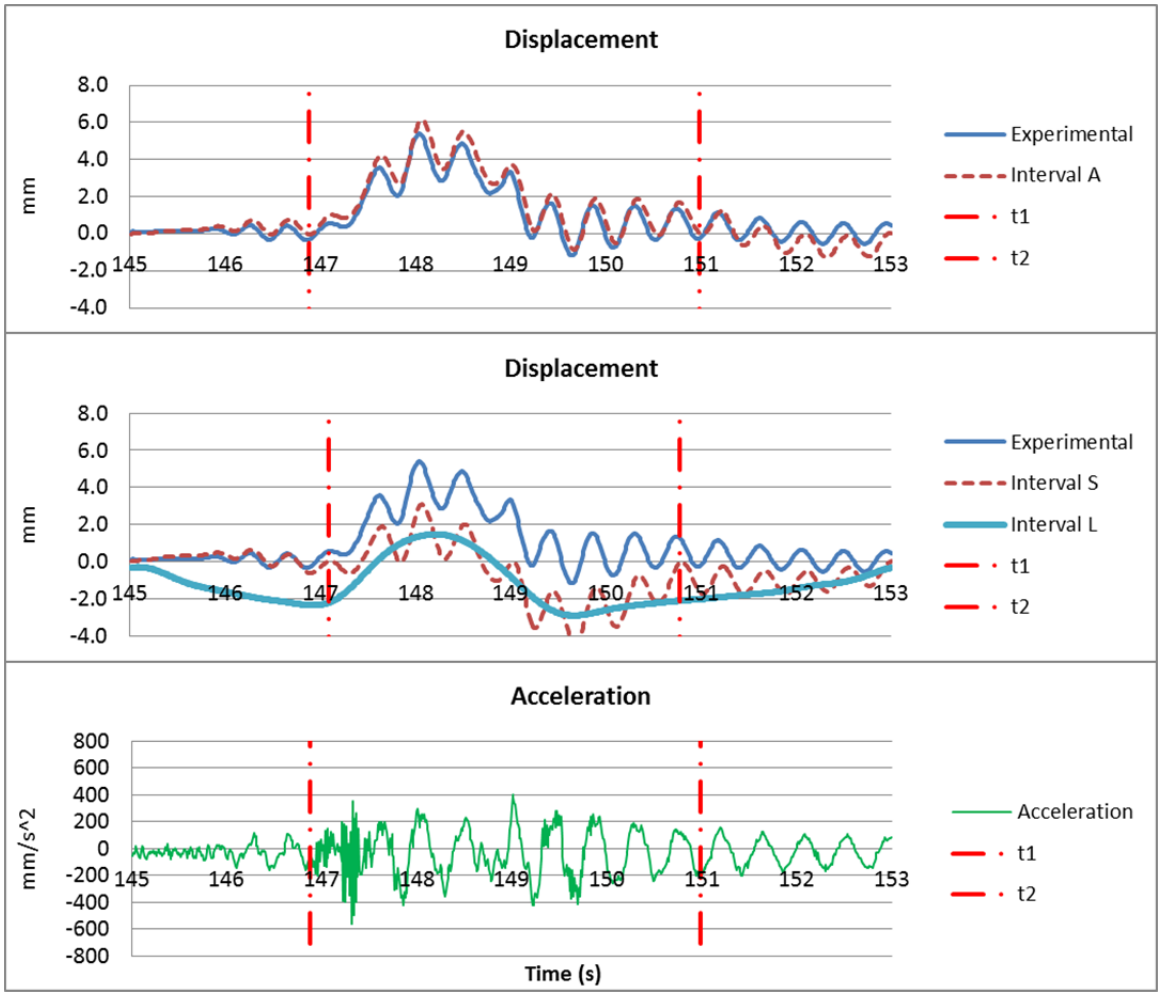

Figure 5.8 Displacement results for Test DP3

5.2.2 Estimation of Girder Velocity

In evaluating the girder velocities, only interval A is used, and the free vibration segments are removed. Inspection of the estimated displacement signals reveals that even when there are glaring errors in the magnitudes of the displacements, the curvatures remain very similar when using Intervals A and S. In the Hackensack Bridge analysis, the estimates using Interval L were computed using a low-pass filter to remove the dynamic effect, so only the pseudo-dynamic response is determined. In the 7A Bridge analysis, however, the correct curvature is preserved even when using Interval L. A

correct curvature implies a correct rate of change, which in turn suggests accurate velocity. Therefore, the accurate displacement estimates using Interval A allow for simple differentiation of displacement to obtain accurate velocity.

The error analysis for velocity is not limited to the comparison of only the peaks. Rather, it is important that the curve be able to predict the values on the LDV time waveform since the algorithm is later used to evaluate the rebar oscillations about the stringer. Because of the oscillation of velocity about a zero value, percent error is not appropriate for analyzing the accuracy of the entire signal. As such, it is only used to evaluate the estimate of the peaks. Lastly, the sign of the velocity is irrelevant; the magnitude is the only required quantity. Therefore, all velocities and errors are taken as absolute values.

Table 5.4 shows the velocity estimates using the differentiation method. The peak velocities range from 5.6 mm/s to 30.3 mm/s. As expected, the errors in peak velocities are noticeably lower than those in the peak displacements, with an average 6.5% compared to 10.4%, respectively. Eq. 5.1 is used to determine the root-mean-square deviation (RMSD). These values help to show how well points on the curve are predicted by the predicted velocity. Another measurement is the mean absolute error in mm/s, which gives the actual differences in the velocity magnitudes as an average. These two measurements actually give similar values. On average, the velocity estimate is within 0.83 mm/s of the LDV results. Since peak velocities are significantly higher than this error, the results are reasonably accurate.

Table 5.4 Summary of estimated girder velocity

Test	Time relative to embedment, minutes	Load duration, sec	LDV peak velocity, mm/s	Error of peak velocity		Mean absolute error, mm/s	Root-mean-square deviation
				mm/s	%		
BP3	-230	4.41	10.0	0.31	3.07	0.42	0.57
BP5	-209	5.29	5.6	0.46	14.24	0.44	0.52
DP3	-105	4.11	24.0	1.24	5.16	1.92	2.23
DP7	-67	3.09	22.5	0.60	3.21	0.67	0.82
DP17	22	3.3	13.4	0.66	4.98	0.62	0.78
DP17	25	3.99	13.1	0.78	7.85	0.43	0.55
DP17	26	3.27	12.1	0.55	4.54	0.66	0.80
DP19	48	3.35	9.6	0.12	2.12	0.51	0.63
DP19	49	3.57	8.5	0.82	10.11	0.58	0.74
DP21	68	2.55	12.6	2.00	15.94	0.87	1.05
DP21	71	3.29	10.8	0.41	3.74	0.39	0.51
AP2	121	3.01	23.3	0.42	2.00	0.78	0.94
AP2	125	3.15	19.5	0.70	3.58	1.16	1.48
AP3	149	3.52	21.1	2.71	16.76	1.71	1.98
AP4	181	3.51	17.1	0.86	5.16	0.66	0.81
AP5	223	4.13	16.6	0.42	2.99	1.03	1.43
AP6	247	3.67	30.3	1.58	5.58	1.28	1.53
Maximum				2.71	16.76	1.92	2.23
Minimum				0.12	2.00	0.39	0.51
Average				0.86	6.53	0.83	1.02

To confirm the notion that accurate velocity estimates will follow from accurate displacement estimates, the errors in the peak values are compared in Figure 5.9. The tests are sorted such that the displacement errors are given in ascending order. It is shown in the figure that the velocity errors are typically much lower than displacement errors.

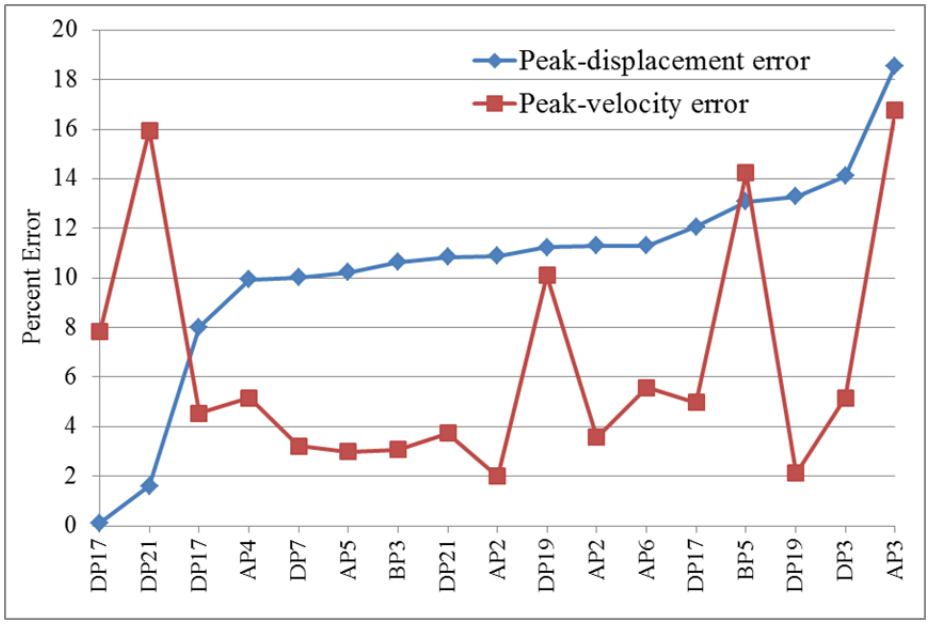

Figure 5.9 Comparison of displacement errors with velocity errors

A typical good result of the velocity estimate is shown in Figure 5.10. The predicted signal closely follows the high frequency curvature of the LDV velocity signal. It should be noted, though, that the velocities are not close to zero in the free vibration segments. While force is required to sustain acceleration, a bridge set into motion with initial velocity may vibrate at a small magnitude of velocity for some time because of inertial laws. Nevertheless, excitation from an external source can be discerned by observing the frequency and amplitude changes at the t_1 boundary line.

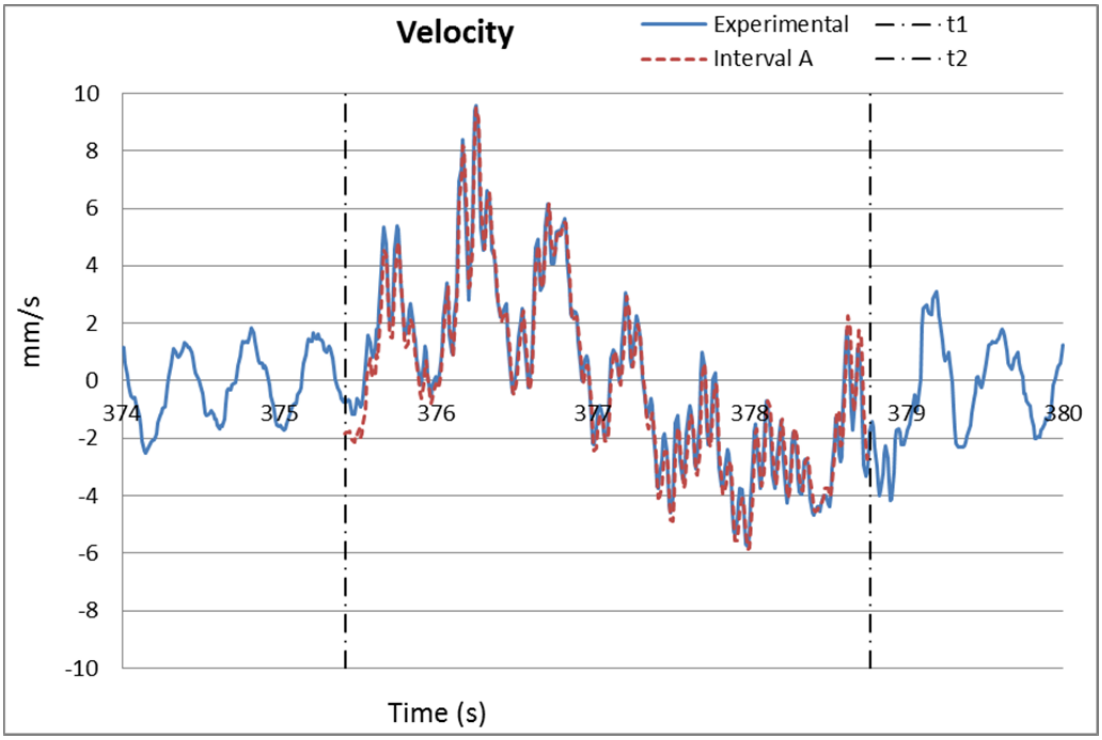

Figure 5.10 Velocity estimate for Test DP19

Figure 5.11 shows the poorest velocity estimate, which actually corresponds to the poorest displacement estimate. The displacement peak from Test AP3 had the highest percent error, 18.6%, among all the tests when using Interval A. The resulting error in velocity is a linear drift with a slope of -0.03 mm/s. Since distortions in the displacement estimate are parabolic, the derivative of displacement should indeed be distorted in a linear manner. For illustration purposes only, a baseline correction is applied by subtracting a line equal to this drift. The velocity histories are then identical in Figure 5.12. It should be noted that none of the estimated velocity records were baseline-corrected in the error analysis. Even without correction, the errors were within reason, and the algorithm was applied to the rebar and stringer with confidence.

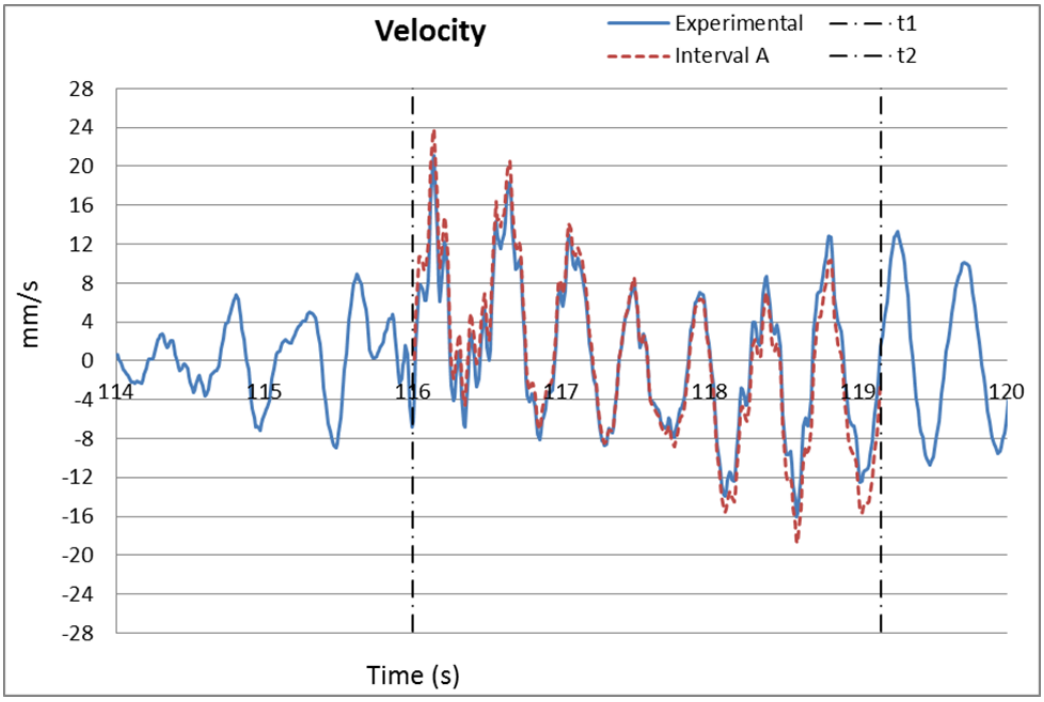

Figure 5.11 Velocity estimate for Test AP3

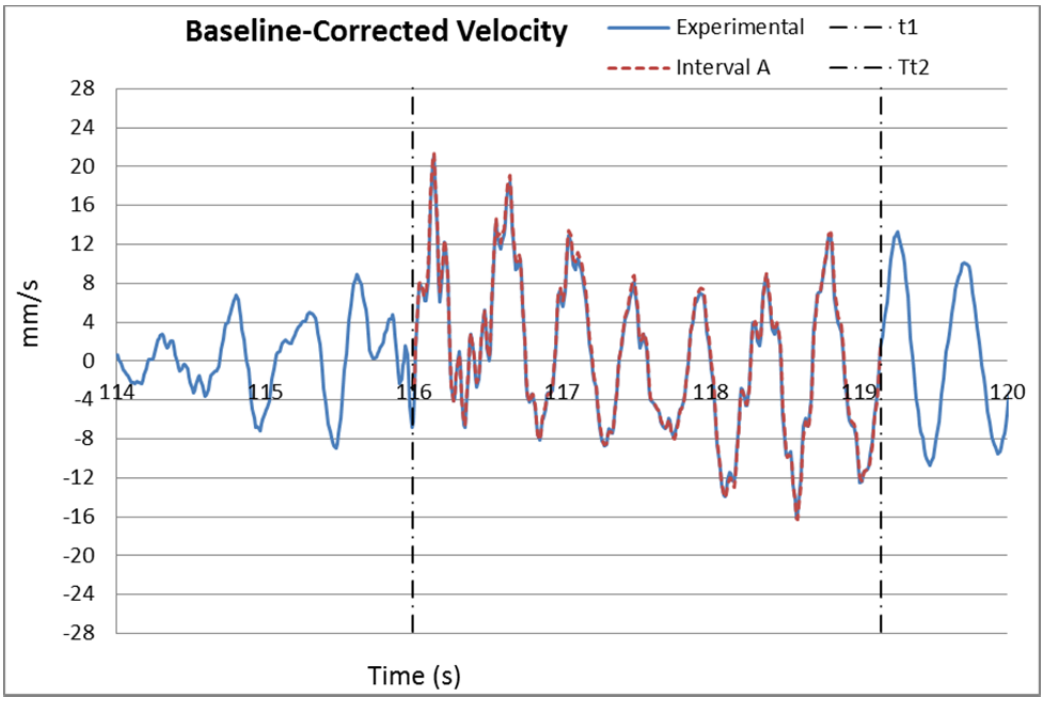

Figure 5.12 Velocity estimate after baseline correction (Test AP3)

5.2.3 Relative Velocity of Deck Reinforcement Bars

Using the parameters, t_1 and t_2, of Interval A from the girder analysis, the conversion algorithm was applied on the rebar and stringer acceleration data (Sensors A2085 and A2084, respectively) to obtain velocity estimates at key times during the deck concrete pour. Table 5.5 gives a summary of measured accelerations and estimated velocities results for the rebar. The max absolute values are the peak values relative to the global frame of reference. The max relative values represent the largest difference between the stringer and rebar responses at any instant in time, as given by the estimated signals. The average relative values give the average difference between data points on the stringer and rebar time waveforms.

Table 5.5 Summary of rebar response

Test	Time relative to embedment	Rebar Acceleration			Rebar Velocity		
		Max absolute	Max relative	Average relative	Max absolute	Max relative	Average relative
	(min)	(mm/s^2)	(mm/s^2)	(mm/s^2)	(mm/s)	(mm/s)	(mm/s)
BP3	-230	985	1038	277	8.34	9.49	2.95
DP3*	-105	1011	1010	227	22.14	9.54	2.14
DP7	-67	1160	1117	263	19.01	11.21	2.56
DP17	22	213	293	83	7.36	3.93	1.02
DP17	25	356	297	81	10.56	4.15	1.15
DP17*	26	270	473	107	9.96	6.45	1.61
DP19	48	225	299	61	4.63	3.09	0.73
DP19*	49	310	348	81	7.18	3.62	0.90
DP21*	68	399	292	64	8.26	2.29	0.56
DP21	71	428	283	58	7.02	3.11	0.47
AP2	121	344	198	49	10.56	1.69	0.46
AP2*	125	379	191	46	9.48	1.91	0.50
AP3	149	399	204	45	9.58	1.74	0.48
AP4*	181	267	159	35	7.41	1.04	0.32
AP5	223	309	231	48	7.75	2.01	0.44
AP6*	247	425	134	33	25.20	1.85	0.69

***** Tests shown in Figure 5.14 Figure 5.20

A trend of decreasing relative accelerations and velocities can be observed from Table 5.5 as time passed from the moment the rebar is embedded in concrete and the concrete began to set. However, the peak velocities due to traffic are inconsistent, and it is important to check that the decreases in the response do not simply follow from the change in traffic over time. Figure 5.13 plots the values of the stringer and rebar peak responses over time, relative to the global reference frame. The third curve represents the maximum response of the rebar relative to the stringer at any point (i.e., not just at the peaks). Lastly, the upper-bound limit of 38 mm/s on peak particle velocity is plotted. From Table 2.1, the appropriate limit for concrete age up to 3 hours is actually 102 mm/s, but 38 mm/s is conservatively selected because it is the lowest value given. Ultimately, it is shown in Figure 5.13 that none of the velocities are even close to this limit.

The figure shows that prior to the pouring of concrete, the stringer response does not fluctuate as much as the rebar response. After $t = 0$, when the rebar is embedded in concrete, the peak absolute accelerations and velocities continue to fluctuate due to different live loads passing over the bridge. Even though the peak absolute responses do not follow any trend, the relative response of the rebar is shown to steadily decrease. This is especially true for the velocity, where a large spike in the absolute velocity at the end of the record (25.2 mm/s at 247 minutes) does not induce a spike in the relative velocity. This demonstrates the setting of the concrete and its effect of constraining the rebar response to that of the surrounding concrete deck, which in turn is constrained to the response of the nearby stringer.

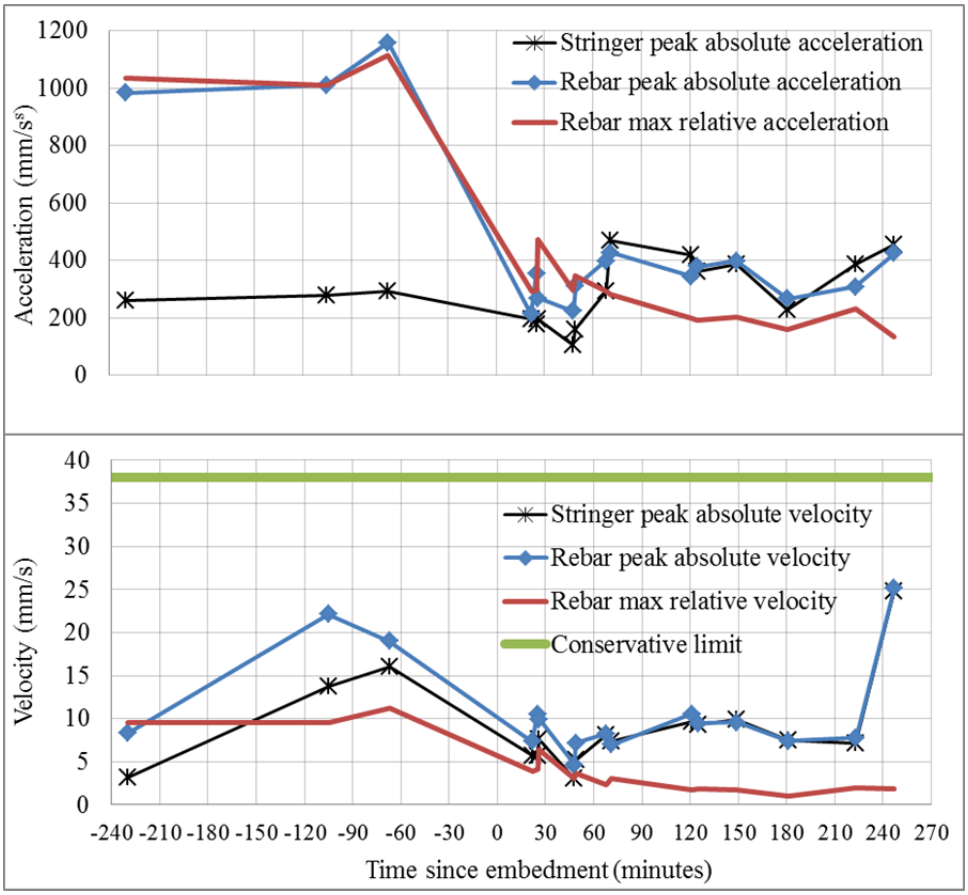

Figure 5.13 Stringer and rebar responses over time

Figure 5.15 through Figure 5.20 illustrate the progression of the rebar and stringer responses over the course of the pouring and setting period. To provide an initial reference, Figure 5.14 shows the typical response prior to the deck pour. The velocity signal of the rebar is clearly shown to oscillate about that of the stringer, signifying relative motion. The displacements are similar to those in Figure 5.8, further validating the velocity estimate.

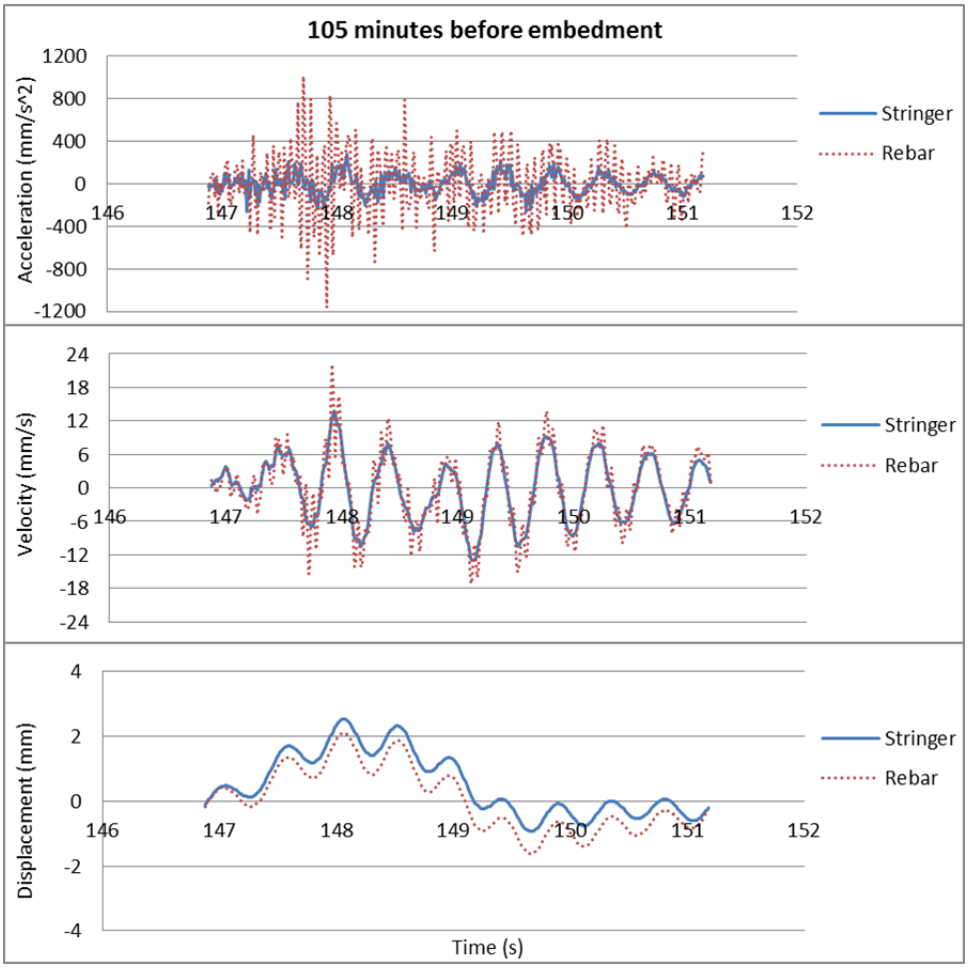

Figure 5.14 Rebar and stringer response for Test DP3

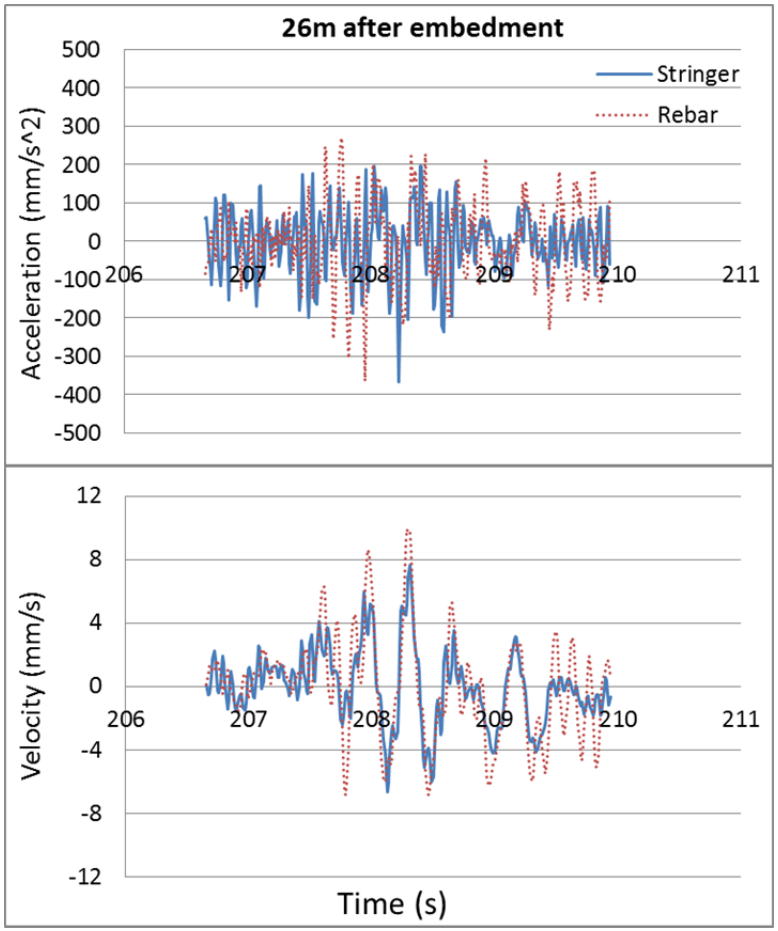

Figure 5.15 Response for Test DP3

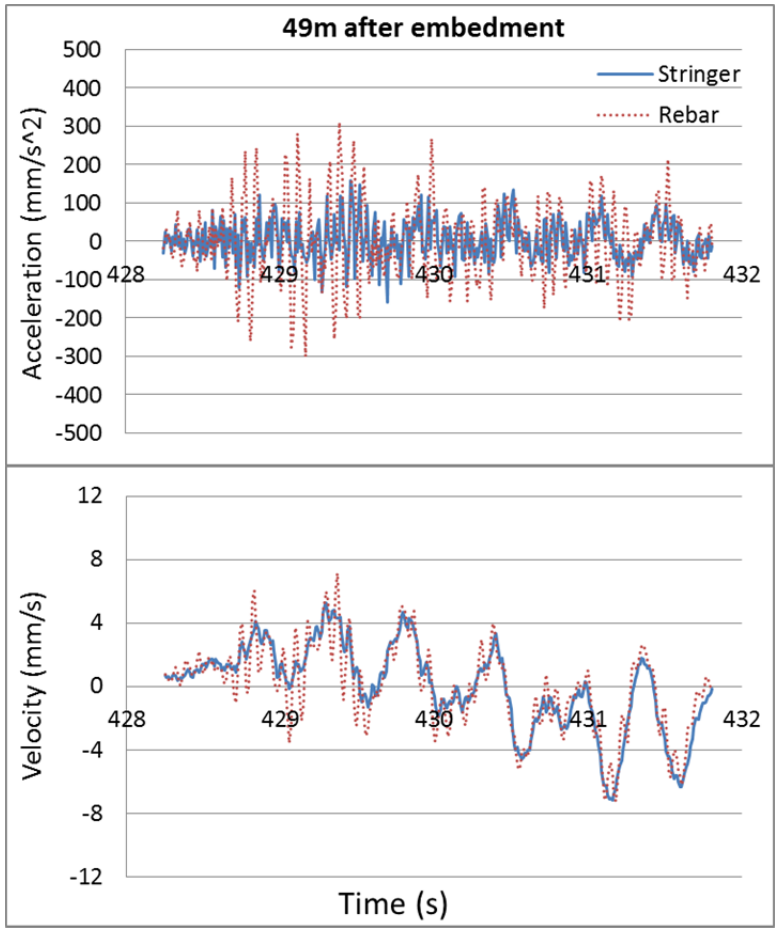

Figure 5.16 Response for Test DP17

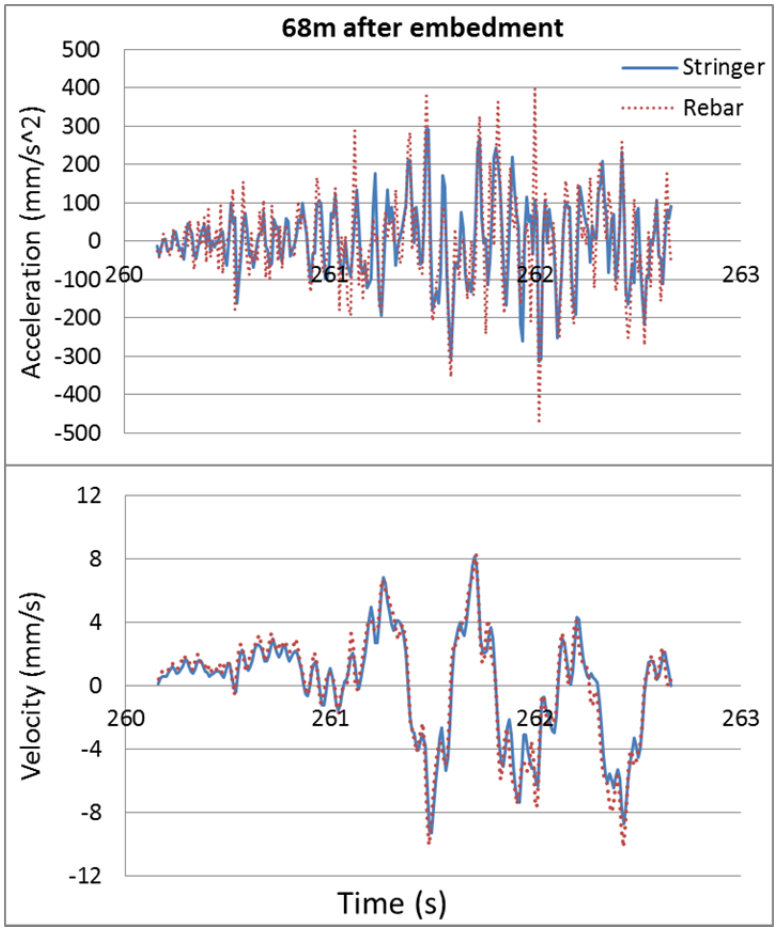

Figure 5.17 Response for Test DP19

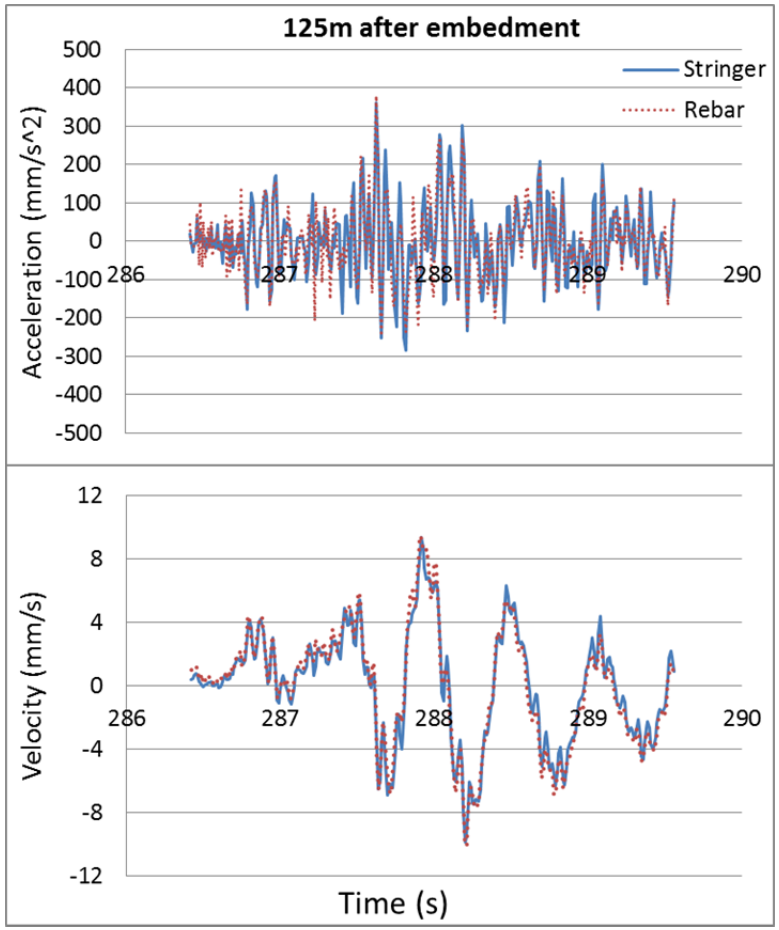

Figure 5.18 Response for Test DP21

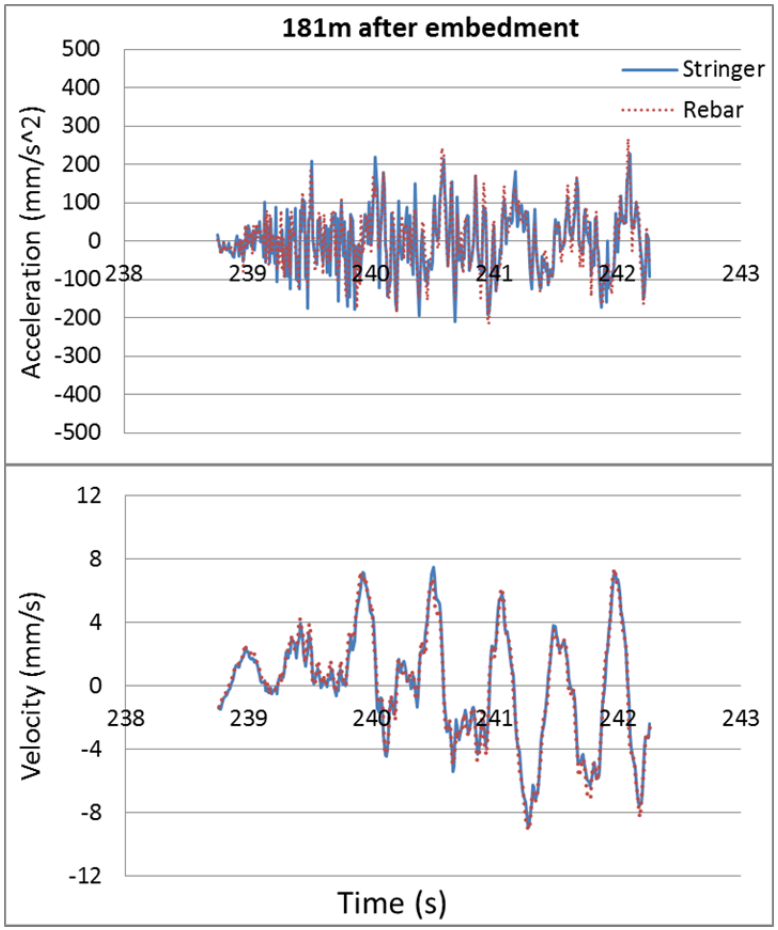

Figure 5.19 Response for Test AP4

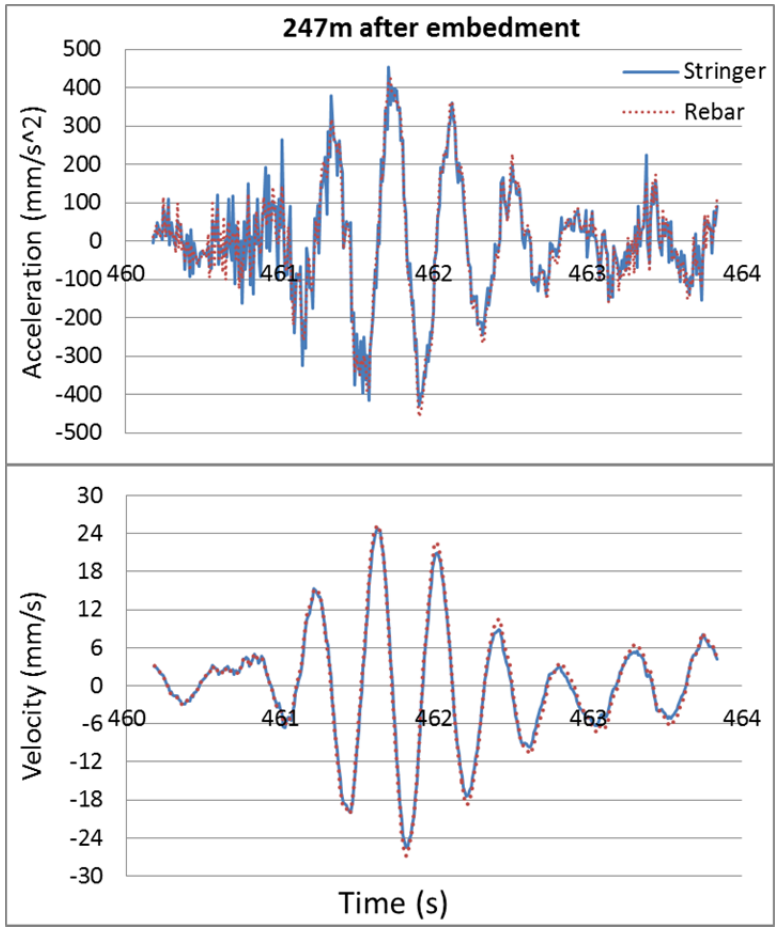

Figure 5.20 Response for Test AP6

When the time reached 26 minutes after embedment, the rebar was still oscillating relative to the stringer. The same was true after 49 minutes. Figure 5.17 shows that at 68 minutes, there is no discernible oscillation. Differences in the rebar and stringer signals occur only at the local maxima and minima, or cusps, on the curves. These small differences can be partially attributed to small errors in the estimated signals. For all practical purposes, however, the stringer and rebar responses after 68 minutes are essentially harmonic. This means that the concrete achieved its initial set between 49 to 68 minutes after placement. The behavior is consistent through the 4 hours after placement, as shown in Figures Figure 5.18 through Figure 5.20.

The established limits on peak particle velocity by Hulshizer and Desai (1984) give 102 mm/s as an upper-bound for the first three hours after placement, and 38 mm/s for the following eight hours. The authors explained that these values were conservative, and additional testing could be used to increase the limits. On the Hackensack Bridge, the limits were never reached. Even during the periods before concrete placement, the bare rebars did not achieve velocities even close to the limit of 102 mm/s, and no observed velocities exceeded the more conservative 38 mm/s limit. Furthermore, the rebar velocities continued to decline as the concrete achieved its initial set. For this bridge, then, there is no evidence of debonding of deck reinforcement resulting from vibrations induced by adjacent live loads.

CHAPTER 6

SUMMARY AND CONCLUSIONS

6.1 SUMMARY

The field instrumentation of the two bridges led to the evaluation of thirty sets of bridge dynamic response data. The NJTA Interchange 7A Bridge was closed to traffic, allowing for a controlled testing program, while the Hackensack River Bridge was evaluated for periods of typical highway traffic. A preliminary investigation was performed to compare deck rebar tiedown conditions from just raw accelerometer data. Then, an algorithm was developed to predict and reconstruct bridge girder velocity and displacement time histories using accelerometer data. The algorithm involved subjective analysis combined with numerical processing. To obtain accurate estimates of the rebar relative velocity, the analysis proceeded systematically in determining the girder displacements, followed by girder velocities, and concluded with the stringer and rebar velocities. These results were compared with allowable limits to determine the severity of the vibration effects due to live loads in adjacent lanes.

6.2 CONCLUSIONS

The findings from the comprehensive evaluation of bridge dynamic response yielded the following conclusions:

(1) The tiedown of every rebar intersection resulted in a marked reduction in the acceleration of the top mat of reinforcement when compared to the tiedown of every other intersection. Mathematically, the factor of reduction in acceleration should result in the same factor of reduction for velocity, so 100 percent tiedowns will help mitigate debonding effects on rebars.

(2) When converting acceleration signals into displacement, the estimated displacements are highly sensitive to the choice of bounds, t_1 and t_2, of the time segment to be converted. Errors due to the approximations of t_1 and t_2 can be reduced by including more of the initial free vibration segments rather than by truncating the forced vibration segment.

(3) For continuous bridges, the estimated response of the first loaded span becomes inaccurate after the vehicle leaves that span. Noise components of the signal dominate the pseudo-static response components. This is partially mitigated by evaluating the acceleration history for only a single loaded span at a time.

(4) The algorithm can be used to process data for normal highway traffic. The response can be evaluated for vehicles traveling at speeds as low as 20 mph, with no practical upper-bound, given that the total time on the span is short (less than 6-8 seconds). The main reservation is that a series of heavy vehicles can obscure the boundaries of forced vibration and introduce unknown initial conditions.

(5) Once the forced vibration segment is identified and the bounds are accurately chosen, the same set of bounds can be used to evaluate multiple

bridge components. The bounds that result in accurate estimates of the girder response, for example, can be used to estimate the responses of floor beams, stringers, and other structural components.

(6) The concrete initial set time is between 49 to 68 minutes, after which the rebar and deck responses are in unison. Induced vibrations after this period should be inconsequential to the rebar bond.

(7) The adjacent traffic loads on the Hackensack River Bridge did not induce sufficient vibration in the rebars to pose any significant risk of debonding with the surrounding concrete.

6.3 FUTURE RESEARCH

The parameters that affect displacement estimates the most are the bounds of forced vibration. A more rational method is desired to determine these precise bounds. Weigh-in-Motion systems, for example, may be able to signal the start and end times of the span loading. By configuring a WIM system with the proper parameters to identify forced vibration, it may be possible to fully or partially automate the conversion of accelerometer data into displacement.

Currently, there is a limited understanding of vibration effects on rebar bond. The effects need to be quantified so that accurate limits can be prescribed. The instrumentation and field testing of other bridges during deck pours can be combined with coring tests to determine what types of loads and responses would cause debonding of reinforcement. Laboratory work can also be done to model the extreme cases of

vibration that can be expected in the field. Then, the actual magnitudes of acceleration, velocity, and/or displacement that cause debonding may be determined.

REFERENCES

Altowaiji, W. A. K., Darwin, D., & Donahey, R. C. (1986). Bond of Reinforcement to Revibrated Concrete. *ACI Journal, 83*(6), 1035-1042.

Arraigada, M., & Partl, M. (2006). *Calculation of displacements of measured accelerations, analysis of two accelerometers and application in road engineering.* Paper presented at the 6th Swiss Transport Research Conference, Ascona, Switzerland.

Boore, D. M. (2001). Effect of Baseline Corrections on Displacements and Response Spectra for Several Recordings of the 1999 Chi-Chi, Taiwan, Earthquake. *Bulletin of the Seismological Society of America, 91*(5), 1199-1211.

Boore, D. M. (2005). On Pads and Filters: Processing Strong-Motion Data. *Bulletin of the Seismological Society of America, 95*(2), 745-750.

Boore, D. M., Stephens, C. D., & Joyner, W. B. (2002). Comments on Baseline Correction of Digital Strong-Motion data: Examples from the 1999 Hector Mine, California, Earthquake. *Bulletin of the Seismological Society of America, 92*(4), 1543-1560.

Chiu, H.-C. (2012). A Compatible Baseline Correction Algorithm for Strong-Motion Data. *Terrestrial, Atmospheric, and Oceanic Sciences, 23*(2), 171-180.

Douglas, B., Maragakis, E., & Nath, B. (1990). Static Deformation of Bridges from Quick-Release Dynamic Experiments. *Journal of Structural Engineering, 116*(8), 2201=2213.

Faulkner, B. C., Barton, F. W., Baber, T. T., & McKeel, W. T. (1996). Determination of Bridge Response Using Acceleeration Data *Report VTRC 97-R5*: Virginia Transportation Research Council.

Gilbert, H. B., Celik, O., & O'Malley, M. K. (2010). *Long-Term Double Integration of Acceleration for Position Sensing and Frequency Domain System Identification.* Paper presented at the 2010 IEEE/ASME International Conference on Advanced Intelligent Mechatronics, Montreal, Canada.

Gindy, M., Nassif, H. H., & Velde, J. (2007). Bridge Displacement Estimates from Measured Acceleration Records. *Transportation Research Record: Journal of the Transportation Research Board, No. 2028*, 136-145.

Han, S., & Chung, J. W. (2002). *Retrieving Displacement Signal from Measured Acceleration Signal.* Paper presented at the IMAC 20th Conference and Exposition on Structural Dynamics, Los Angeles, California.

Harsh, S., & Darwin, D. (1986). Traffic Induced Vibrations and Bridge Deck Repairs. *Concrete International: Design & Construction, 8*(5), 36-42.

Hulshizer, A. J., & Desai, A. J. (1984). Shock Vibration Effects on Freshly Placed Concrete. *Journal of Construction Engineering and Management, 110*(2), 266-285.

Nassif, H. H., Davis, J. C., & Suksawang, N. (2007). Evaluation of Bridge Deck Cracking on the Delaware River Turnpike Bridge (Structure No. P0.00): Final report submitted to the New Jersey Turnpike Authority.

Park, K.-T., Kim, S.-H., Park, H.-S., & Lee, K.-W. (2004). The determination of bridge displacement using measured acceleration. *Engineering Structures, 27*, 371-378.

Paultre, P., Proulx, J., & Talbot, M. (1995). Dynamic Testing Procedures for Highway Bridges Using Traffic Loads. *Journal of Structural Engineering, 121*(2), 362-376.

Ribeiro, J. G. T., Castro, J. T. P., & Freire, J. L. F. (2002). *Filtering in Frequency Domain to Avoid Time Aliasing.* Paper presented at the IMAC 20th Conference and Exposition on Structural Dynamics, Los Angeles, California.

Ribeiro, J. G. T., Freire, J. L. F., & Castro, J. T. P. (1999). *Some Comments on Digital Integration to Measure Displacements using Accelerometers.* Paper presented at the IMAC 17th International Modal Analysis Conference, Kissimmee, Florida.

Shreve, D. H. (1995). Signal Processing for Effective Vibration Analysis. *IRD Mechanalysis, Inc.*